TECHNISCHE UNIVERSITÄT WIEN
Vienna University of Technology

DIPLOMARBEIT

Development and Testing of a Sr-Measurement System for Integration in an existing vertical I-V-Measurement System

Ausgeführt am

Atominstitut

der Technischen Universität Wien

unter der Betreuung von

Ao.Univ.Prof. Dipl.-Ing. Dr.techn. Johann Summhammer

und durchgeführt bei

Dipl.-Ing. Dr. Stephan Abermann

am AIT Austrian Institute of Technology GmbH

durch

BSc., Michael Revesz

Matr. Nr. 0626920

Johann-Laufner-Gasse 41/18

1210 Wien

AUSTRIA

Wien, am 25. März 2014

Danksagung

Ich möchte mich beim Austrian Institute of Technology für deren Unterstützung bei meiner Arbeit bedanken, auch bei den Kollegen im Photovoltaics Departement und im Besonderen bei Stephan, Bernhard und Gerhard, für deren Unterstützung.

Bei meinen Eltern möchte ich mich für deren finanzielle Unterstützung und den Ansporn bedanken.

Vielen Dank auch an Sînzi für ihre Geduld und Aufmunterung.

Contents

List of Figures

List of Tables

Abstract

The aim of this work was to evaluate different methods for Sr-measurement and to develop and construct a measurement system which can be integrated inside a vertical I-V-measurement system and be used for the measurement of commercial sized PV-modules at AIT Austrian Institute of Technology GmbH. In addition the Sr-measurement system is supposed to perform a measurement according to the standard IEC 60904-8. The most promising possibilities for achieving quasi-monochromatic light are shortly discussed in this work. Afterwards the developed Sr-measurement system is introduced and the different components are explained. This system is based on optical bandpass filters, used for producing quasi monochromatic light and the lamp used for illumination is a Xenon flasher. Achieving a large area with homogeneous irradiation within ± 2 % is impossible with this set-up as it is, only ± 5 % can be achieved for large area modules. Very small modules can be measured under the strict conditions for homogeneity. In addition, leaking white light is disturbing the Spectral Response-measurement, thus overcoming any other measurement error. Therefore, the system can not yet be used for a serious Spectral Response-measurement and for measurements under normative regulations. However, this system is a first prototype which has to be and can be improved. Furthermore, this system has potential to be extended, e.g. for use with other PV-module technology such as multi-junction devices after installing coloured bias light.

Kurzzusammenfassung

Das Ziel dieser Arbeit war mehrere Methoden zur Messung der Spektralen Empfindlichkeit (Sr) zu beurteilen und anschließend ein Messsystem zu entwickeln und zu bauen, welches in ein bestehendes vertikales I-V-Messsystem integriert werden kann. Zudem soll es zur Messung von PV-Modulen in handelsüblicher Größe am AIT Austrian Institute of Technology GmbH geeignet sein. Zusätzlich sollen die Sr-Messungen nach IEC-Norm 60904-8 durchgeführt werden können. In dieser Arbeit werden zunächst die am besten geeigneten Möglichkeiten kurz diskutiert, um quasi-monochromatisches Licht zu erzeugen. Anschließend wird das im Rahmen dieser Arbeit entwickelte Messsystem vorgestellt und die einzelnen Komponenten erläutert. Das quasi-monochromatische Licht wird bei diesem Messsystem durch optische Bandpass-Filter erzeugt. Dabei dient eine Xenon-Blitzlampe als Lichtquelle. Mit dem derzeitigen Aufbau kann eine Homogenität der Strahlungsleistung auf Modulebene innerhalb von ± 2 % für große Modulflächen nicht gewährleistet werden, eine Homogenität innerhalb von nur ± 5 % jedoch schon. Sehr kleine Module können trotzdem unter den strengen Kriterien, die an die Homogenität gestellt werden, vermessen werden. Zusätzlich besteht noch das Problem, dass weißes Licht von der Lichtquelle in den Messraum eindringen kann und damit das quasi-monochromatische Licht bei der Messung der spektralen Empfindlichkeit stört. Dadurch kommt es zu Messfehlern, die die sonst üblichen Fehler weit überragen. Deshalb kann dieses Messsystem derzeit nicht für vernünftige Messungen der spektralen Empfindlichkeit benutzt werden und im speziellen auch nicht für Messungen unter Norm-Auflagen zur Zertifizierung. Dennoch konnte recht erfolgreich ein erster Prototyp entwickelt werden, der noch verbessert werden kann und muss. Zusätzlich besteht für dieses System Potential, da es z.B. durch Erweiterung mit farbigem BIAS-Licht zur Vermessung anderer PV-Modultechnologien wie Multijunction-Modulen geeignet ist.

Chapter 1.

Introduction

The Spectral Response (Sr) (also often referred as Quantum Efficiency (QE)) of a PV-module or a solar cell is one of the most important and measurable properties. On the one hand it provides information about material properties or processes and helps understanding the mechanisms. A few examples are the optical loss due to reflection, generation of charge carriers and absorption inside the material, diffusion or diffusion length, or the process of recombination [12], [13]. On the other hand, amongst other reasons, it is an important quantity for the spectral correction factor which is used for solar cell or module calibration [13] and it can be used to judge the suitability for a specific location. Therefore it is important to know the Sr of photovoltaic devices and to measure this quantity. The aim of this work is to evaluate different methods for Sr-measurement and to develop and construct a Sr-measurement system. Further more this system is supposed to be integrated inside a vertical I-V-measurement system and to be used for the measurement of commercial sized PV-modules at AIT Austrian Institute of Technology GmbH. In addition the Sr-measurement system should be able to perform a measurement according to the standard IEC 60904-8, “Photovoltaic devices - Part 8: Measurement of spectral response of a photovoltaic (PV) device”.

Chapter 2.

Theory

2.1. Physics of Solar Cells

[1] In general solar cells are devices that show the photo-electric effect. This means, photons, which are incident on the solar cell, transfer their energy to charge carriers inside the material of the solar cell and the charge carriers are being excited to the conduction band of the material. Thus, the charge carriers are able to move freely and the solar cell can be used as a current source. However, those created charge carriers can not easily be used or extracted. Their movement is affected by many effects, of which the most important and basic ones will be discussed in the following chapters.

2.1.1. Charge Carrier Separation and Junctions

The collection of the created charge carriers and its transport out of the device as well as the charge separation is done via the junction. The charge separation can be achieved by a spatial variation of either the band gap, the electron affinity or a gradient in the vacuum level [14]. This can be done inside the semiconductor itself by changing its composition or by bringing a semiconductor in contact in between other materials. Last arrangement is called a hetero-junction. Another method to get a spatial gradient in the vacuum level is by varying the doping density in a semiconductor [14]. All of those methods create an electrical field that attracts the electrons to one side of the device and pushes the holes to the opposite side. Thus, a net current or a difference in potential along the device are created.

[1] The chapter 2.1 is partially taken from a literature review with the title “Selection Of Developments For Solar Cells Using Quantum Dots” and is written by me (Michael Revesz) in 2011 at University of Loughborough.

There are two types of semiconductors classified by their doping. The one is doped with elements that carry more electrons in their valence band than necessary for the binding in the crystal. These excess electrons are then filling the conduction band and enhance conductivity. As the carriers are of negative charge these semiconductors are called n-type and its impurities behave as electron *donors*. On the other hand the impurity atoms can carry less electrons than necessary for the valence bonds of the main atoms in the crystal. Therefore those impurities provide holes as the charged carriers for conduction. As the holes are positive charged these semiconductors are of p-type and the impurity atoms are called electron *acceptors*. An un-doped semiconductor is called intrinsic.

In order to extract and separate the electron hole pairs created by the photovoltaic effect from the semiconductor where they have been created, an electric field is required. This field can be created by a junction of either the same semiconductor but of different doping type or a hetero-junction [14]. The latter is a junction of two different materials. One example for the first type of junction is a p-n junction, i.e. a junction of a p-type semiconductor and a n-type semiconductor. A second junction for this type is the p-i-n junction. This is an intrinsic layer between a p- and a n-type semiconductor. These two junctions are the ones usually used in photovoltaic devices.

In order to explain the mechanism for charge separation, one can consider a simple p-n junction. First an equilibrium state without additional carrier creation is assumed. When the two semiconductors are brought together, one gets free electrons in the conduction band on the n-type side of the device. On the n-side there are unfilled valence bands. So just in a closer region of the junction the free electrons of the donors move, by diffusion, to the acceptors which are likely to get an electron to satisfy the number of binding in the crystal. Thus, the p-side is getting negative charged and the n-side positive charged. In equilibrium the charge density is equal on both sides and an electric field is created in this charged region. This can be seen in figure 2.1. The other part of the semiconductor remains uncharged. When a neutral pair of a hole and an electron reaches this charged region by diffusion [15] the electric field behaves attractive to electrons, separates them from the holes and pushes them to the p-doped semiconductor. The reverse happens with holes coming from the p-doped side. In the case of a p-i-n junction the electric field goes along the whole intrinsic semiconductor as it remains uncharged. Typical layouts of p-n and p-i-n solar cells are shown in figure 2.2. So in a p-n device the light absorption is meant to take place mainly in the p-type layer which has to be thick enough to allow sufficient light absorption. Whereas in a p-i-n device light is absorbed and the carriers are created in the intrinsic layer. Therefore

in a p-i-n device the intrinsic layer has to be thick enough and the p-layer can be thin again in order to reduce material. In this case the p-layer works as a collector for the holes. In both cases the n-layer has to be thin enough to allow photons to pass through it and enter the main layer of the device.

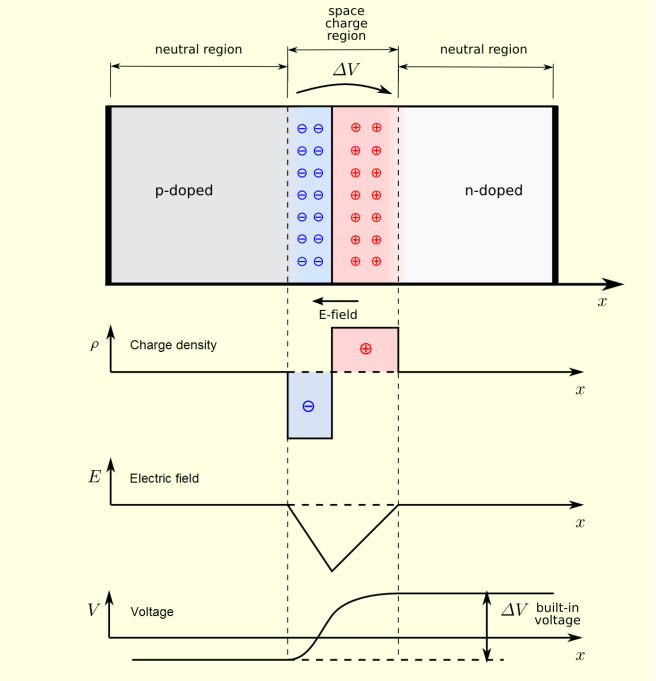

Figure 2.1.: p-n junction without bias [1]

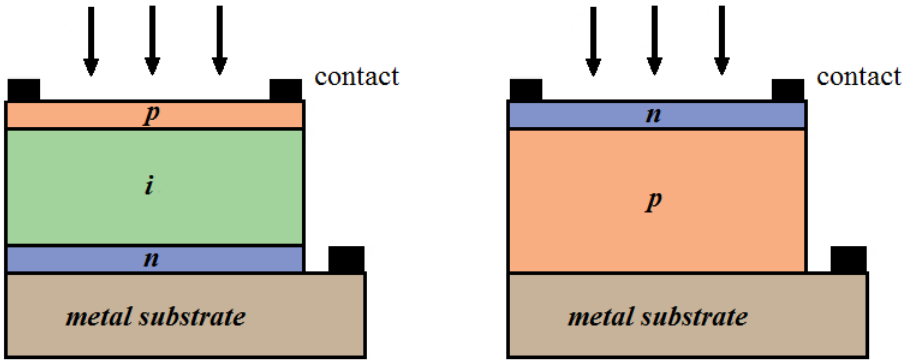

Figure 2.2.: Schematic solar cells: left as p-i-n junction, right as p-n junction

2.1.2. Effect of Impurities - Doping

In intrinsic semiconducting materials the energy levels are determined by the overlap of the atomic orbitals with the crystal bands [14]. Impurities in a crystal lead to a local change in energy levels due to the different bond strength [14]. If occupied energy levels, which are introduced by the impurity, lie within the band gap and above Fermi level, then the Fermi level is increased and therefore in equilibrium the density of electrons is increased compared to the density of holes [14]. Are the unoccupied levels introduced by an impurity below the Fermi level, then the Fermi level is reduced and therefore the density of electrons compared to the density of holes [14]. Semiconductors that act as a electron donator are called n-type semiconductors, converse those that act as electron acceptor are called p-type. Thus, doping influences the conductivity of a semiconductor, even in equilibrium. It has to be mentioned that intrinsic impurities, e.g. crystal defects, cause a change in carrier density and therefore influence the conductivity. An important group of material are the amorphous crystals. These appear as “perfect” crystals in short range, but in long range they have many voids and broken bonds [14].

The carrier densities under bias, e.g. photon flux that creates bias in the solar cell, have the following relation to the energy levels:

$$n \sim e^{-(E_c - E_{F_n})/(k_B T_n)} \tag{2.1}$$

$$p \sim e^{-(E_{F_p} - E_v)/(k_B T_p)} \tag{2.2}$$

where E_{F_p}, E_{F_n} are the quasi Fermi levels with $E_{F_n} - E_{F_p} = \Delta\mu$, as the Fermi level splits under bias [14]. Because under bias the states are supposed to be in a local equilibrium, both are dependent on position. E_v is the valence band level, E_c is the conducting band level and T_n and T_p are the hole and electron “effective temperatures” [14]. The effective temperatures can be understood in the following way: Under bias, when the bias and with it the densities are not changing too fast, the state can be seen as in a local equilibrium as stated above. The only difference is that now holes and electrons have different effective temperatures [14]. For crystalline solids without diffusion and drift, caused by external fields, the total current density is then locally

$$\vec{J}(\vec{r}) = \vec{J}_n(\vec{r}) + \vec{J}_p(\vec{r}) \tag{2.3}$$

with

$$\vec{J}_n(\vec{r}) = \mu_n n \nabla_{\vec{r}} E_{F_n} \tag{2.4}$$

$$\vec{J}_p(\vec{r}) = \mu_p p \nabla_{\vec{r}} E_{F_p} \tag{2.5}$$

where μ_n and μ_p are the electron and hole mobility [14].

The photo-current density under illumination at short circuit is

$$J_{sc} = q \int b_s(E)\, QE(E)\, \mathrm{d}E \tag{2.6}$$

with $QE(E)$ being the cell's **q**uantum **e**fficiency, which is the probability for a photon of energy E delivering one electron to the circuit [14]. b_s is the incident photon flux density per unit area for photons with energy in range of E to $E + \mathrm{d}E$ [14].

In order to demonstrate the basic equations for solar cells, in the following an ideal diode without recombination losses of carriers is assumed. However, resistance at contacts will be considered in the equations. Two types of ohmic resistivity have to be distinguished which causes power to dissipate in a photovoltaic device: Series resistance denoted as R_s and shunt resistance denoted as R_{sh}. The origin of series resistance are the semiconductor-metal contact and ohmic resistance in the metal of the contacts and the semiconducting material. Shunt resistance is mainly caused by leakage of currents along the edges of the device [15]. But also defects at the p-n junction can lead to weak parallel resistance [15]. These are called parasitic resistances. [14] The equation describing the absolute value of the current density in a diode is [14]

$$J = J_{sc} - J_0 \left(e^{\frac{q(V+JAR_s)}{mk_BT}} - 1 \right) - \frac{V + JAR_s}{R_{sh}} \tag{2.7}$$

where A is the solar cell area and m is the ideality factor of the cell, with $m = 1$ for an ideal cell. In real solar cells typical values for m lie between 1 and 2 [14].

In order to describe the photo-current of an illuminated solar cell, we introduce three factors describing the photon flux on a solar cell device. In all three cases we take the flux normal to the surface. It is assumed that radiation is always received from one hemisphere and the surface is considered to be flat. The incident **spectral** flux of photons from the sun normal to the surface is:

$$b_s(E) = \frac{2\pi}{h^3 c^2} \left(\frac{E^2}{e^{\frac{E}{k_B T_s}} - 1} \right) \tag{2.8}$$

with T_s being the temperature of the sun. In addition incident flux of **thermal** photons normal

to the surface has to be considered, too:

$$b_a(E) = \frac{2\pi}{h^3c^2}\left(\frac{E^2}{e^{\frac{E}{k_BT_a}}-1}\right) \tag{2.9}$$

T_a is the temperature of the ambient light. The photon flux from spontaneous emission which results from increased chemical potential $\Delta\mu > 0$ of parts of the electrons due to illumination is:

$$b_e(E,\Delta\mu) = F_e\frac{2n_s^2}{h^3c^2}\left(\frac{E^2}{e^{\frac{E-\Delta\mu}{k_BT_a}}-1}\right) \tag{2.10}$$

n_s is the refractive index of the front material and n_0 is the refractive index of the surrounding medium, so usually air, but is different for application in space. In equation 2.10 $F_e = \pi\frac{n_0^2}{n_s^2}$. For earth application with air as surrounding medium $n_0 = 1$ and therefore $F_e n_s^2 = \pi$. [14] Then the net current density of the solar cell is:

$$J(V) = q\int_0^\infty \Big(1-r(E)\Big)a(E)\left[b_s(E) - \Big(b_e(E,qV) - b_e(E,0)\Big)\right]\mathrm{d}E \tag{2.11}$$

where V is the applied bias (Voltage), $a(E)$ is the probability of absorption and $r(E)$ is the probability of reflection of a photon with energy E and $b_e(E,0)$ corresponds to $b_a(E)$ [14].

The power density of the incident light can be calculated with:

$$P_s = q\int_0^\infty Eb_s(E)\,\mathrm{d}E \tag{2.12}$$

and then the power conversion efficiency at a certain bias and current density is:

$$\eta = \frac{VJ(V)}{P_s} \tag{2.13}$$

To get the maximum power, the device has to be operated at an optimum operation point with bias V_m. This operating point is achieved by maximising the power $VJ(V)$. So

$$\frac{\mathrm{d}}{\mathrm{d}V}\left(VJ(V)\right) = 0 \tag{2.14}$$

Then the maximum efficiency of a cell at the operating point is defined by

$$\eta_m = \frac{J_m V_m}{P_s} \tag{2.15}$$

Here J_m is the photo-current density at the operating point of the cell and
V_m is the correspondent open circuit voltage at the operating point as described above. [14] It has to mentioned that for better light absorption a high optical depth is required. So with increasing the thickness of the absorbing layer [14] the optical thickness is increased as well.

2.1.3. Generation and Recombination Mechanism

There are three types of carrier generation which differ in the type of energy that excites an electron. Two of them are lattice vibrations (phonons) and kinetic energy by carrier collisions. They are thermal excitations. The third one is the excitation by photons which is the essential mechanism for solar cells, even from the point of impact on carrier generation. When an electron is lifted from the valence band to the conduction band then two carriers are created, an electron and a hole. Further more as in a doped material local energy levels exist between the two bands, raising an electron from the valence band to a local level creates a hole and from a local level to the conduction band creates an electron [14].

The three mechanisms of carrier generation are reversible and in the reverse case they are called recombination [16]. When an electron decays to a lower energy level, under recombination with a hole, energy is released. The energy can be released by emitting photons (radiative), by exciting lattice vibrations (non-radiative) which is nothing else than dissipation of heat or by Auger-recombination where a third particle becomes excited by the kinetic energy but is not raised to another band. The latter two mechanism are thermal recombination processes. In thermal equilibrium the rate of thermal recombination is equal to the rate of thermal creation [16].

2.2. The Spectral-Response-measurement

One of the various characteristics of a solar cell or photovoltaic (PV)-module (besides I-V-characteristics) is the Quantum Efficiency (QE). It can be understood as the efficiency

of a PV-cell or any related device to convert incident photons into electrons which can be extracted from the device as an electrical current. Its equation for incident monochromatic light with the wavelength λ is:

$$QE(\lambda) = \frac{n_q}{n_{ph}} = \left[\frac{1}{1}\right], \tag{2.16}$$

where n_q is the total number of created charge carriers and n_{ph} is the total number of incident photons. Another interpretation of the QE is to see it as the probability for an incident photon to be converted into a free charge carrier or electron. This becomes more clear when looking at the equations 2.6 and 2.11 (both taken from [14]). Furthermore, in addition to this definition of QE, also referred to as the external QE, there is the definition of the so called internal QE. The equation for the internal QE is the same as above except in this case the number of photons absorbed by the photovoltaic cell, i.e. not reflected ones, is used [17]. Using probabilities for reflection and absorption then the internal and external QE are:

$$IQE(\lambda) = A$$
$$EQE(\lambda) = (1-R)\cdot A,$$

where R is the probability for a incident photon to be reflected from the surface and A the probability for being absorbed by the material after passing the surface area. As one can see in figure 2.3 the QE for an ideal photovoltaic cell is equal to $100\ \%$, i.e. per incident photon one electron-hole-pair is created, for photons with energy greater then the bandgap E_g of the semiconductor. For photons with energy less then the bandgap the QE is $0\ \%$. Where ever it is written QE only the external Quantum Efficiency is meant.

However, since the QE is not directly measurable another quantity is defined: The Spectral Response (Sr). When illuminating a PV-cell (or similar device) with monochromatic light of one wavelength λ with irradiance $P(\lambda)$[2] and measuring at the same time the electrical output current I of the device then it can be calculated by the equation:

$$Sr(\lambda) = \frac{I}{P(\lambda)} = \left[\frac{\mathrm{A}}{\mathrm{W}}\right] \tag{2.17}$$

As in measurement one usually doesn't have exactly monochromatic light but light with sig-

[2] value of the incident $P(\lambda)$ on the surface area of the PV cell or module

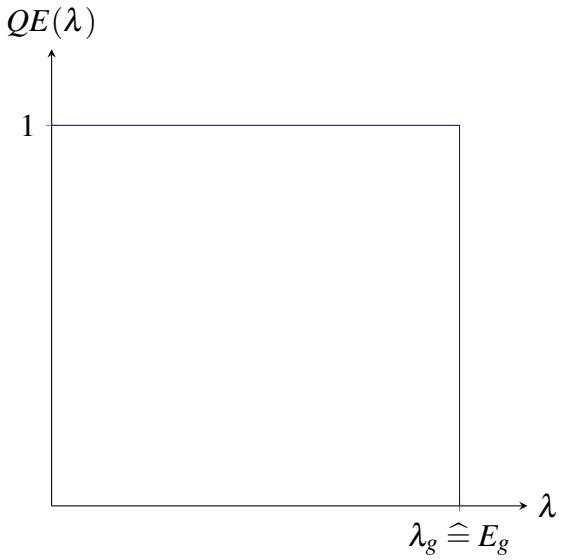

Figure 2.3.: QE of an ideal PV cell

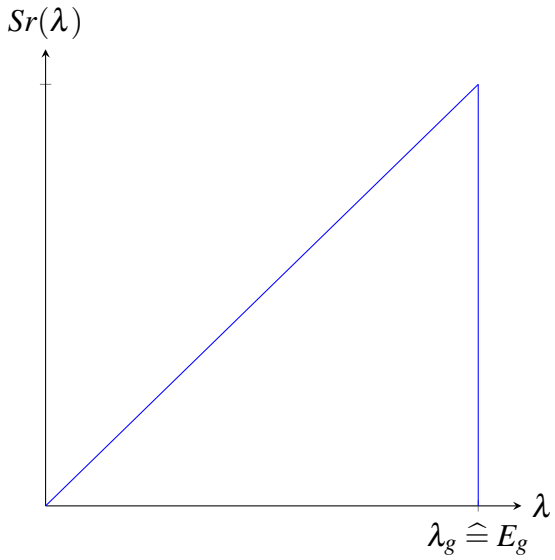

Figure 2.4.: Sr of an ideal PV cell

nificant higher irradiance in the spectrum between $\lambda_0 - \delta$ and $\lambda_0 + \delta$ the

$$Sr(\lambda_0) \approx \frac{\int_{\lambda_0-\delta}^{\lambda_0+\delta} j(\lambda)\mathrm{d}\lambda}{\int_{\lambda_0-\delta}^{\lambda_0+\delta} p(\lambda)\mathrm{d}\lambda}. \tag{2.18}$$

In practice the Sr is approximately the measured current divided by the measured quasi-monochromatic irradiance incident on the module or cell size.

Since the Sr and the QE are equivalent they can be converted into each other by the equation [18]

$$Sr(\lambda) = \frac{q\,\lambda}{h\,c} \cdot QE(\lambda). \tag{2.19}$$

In figure 2.4 one can see the graph of the ideal Sr. Since photons with $\lambda \to 0$ have an energy of $E \to \infty$ and therefore also its irradiance $P(\lambda) \to \infty$ only $n \to 0$ photons fit into a pack with irradiance 1 W. As a consequence the electrical current output $I = 0$ A. This is the reason for $Sr(0\ \mathrm{nm}) = 0\ \frac{\mathrm{A}}{\mathrm{W}}$ and the ideal curve for Sr being a straight line until it reaches its maximum at $\lambda = \lambda_g$. [18] However, for real PV-cells both the QE- and Sr-curves are below the ideal curves. At longer wavelengths for example the absorption is less. Thus, photons are either not absorbed at all or they recombine after they are absorbed too far away from the junction which is collecting the charge carriers ([18], p. 48). In general there are many effects influencing the performance and therefore the QE or Sr. This is the reason why knowledge of QE is so important. It provides information about material properties and processes and

it helps understanding the occurring mechanisms. Amongst those are e.g. the optical loss due to reflection, generation of charge carriers and absorption inside the material, diffusion or diffusion length, or the process of recombination [12], [13].

In principle the Sr-measurement is a simple procedure: A PV-module or cell is illuminated with monochromatic light of known wavelength. Since the irradiance on the device-area has to be known it is measured by a reference cell. The current-output under illumination is simply measured with an ampere-meter. Ideally the measurement should be performed under operation conditions[3] to keep it comparable for customers. However, usually the measurements are performed at short-circuit current since it is more complicated to set the system to operation condition which is different for different devices. This simplification is possible as the Sr is independent of the voltage for most PV-cell types. One example where voltage dependence occurs are amorphous silicon cells. [12] An example set-up for such a measurement system is shown in figure 2.5. In this figure the mount of test-device and reference cell is shown for the case of a PV-cell and has to be adopted for the case of a PV-module. However, the other parts of the system can be used as is or as a similar set-up.

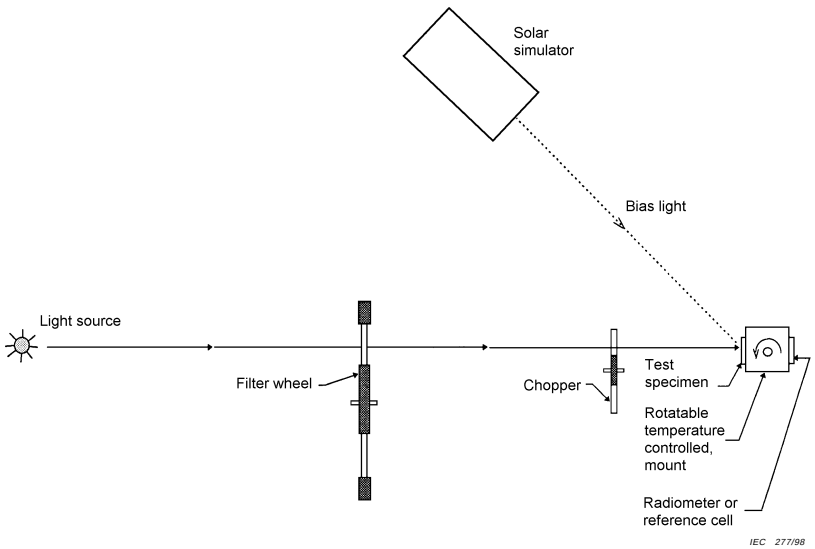

Figure 2.5.: Setup for Spectral Response measurement using a filter wheel [2]

Differences to the latter operational mode apply to multi-junction devices. For those a research group around Mauro Pravettoni consisting of members at the University of Applied Sciences and Arts of Southern Switzerland, the Institute for Energy at the DG Joint Research

[3] operation condition is usually the maximum power point

Centre in Ispra and other Institutions proposed and investigated methods with bias voltage due to the effect of low shunt resistances. Their results have been published e.g. in [19]. In the case of multi-junction devices one needs to bias the junction whose Sr is not measured with coloured light, thus the current output is higher than for the junction to be measured. Thus, to measure the top-junction of a dual-junction device, the bottom one needs to be illuminated with red spectrum, and in the opposite case with blue spectrum respectively. Then the junction to be measured will be current-limiting due to much less irradiation incident on that one. However, when the module is measured at I_{sc} then the measured junction will be in reverse bias voltage [20]. Therefore, forward bias voltage will be necessary in order to bring the junction to be measured to a state with I_{sc} [20]. For finding the correct biasing it is recommended to vary both the light bias and the voltage bias until the Sr reaches its maximum [20], [19].

2.3. Real Spectral Response curves

Before, in chapter 2.2, the ideal Sr curves have been shown. Here, the real curves of a few different solar cell types will be shown and briefly discussed. A comparison of typical spectral response of different solar cell types can be seen in figure 2.6. There the different band-gaps of the different solar cell materials are very well visible. Those are the points where the Sr drops at long wavelengths to $\approx 0\ \frac{\mathrm{A}}{\mathrm{W}}$. The three curves for crystalline silicon or multi-crystalline silicon have the lowest band-gap of around 1.1 eV [14] ($\widehat{=}1130$ nm)[4], CdTe has a band-gap of around 1.44 eV [14] ($\widehat{=}860$ nm) and amorphous silicon has a band-gap of around 1.7 eV [14] ($\widehat{=}730$ nm).

Furthermore, in figure 2.6 a), one can see another important fact: Except for the very short wavelengths, the Sr-curve of float-zone silicon (very pure and perfect crystalline structure) almost looks like the ideal Sr-curve as seen in figure 2.4. All other curves, especially the ones of CdTe and amorphous silicon, but also multi-crystalline silicon, strongly differ from the ideal curve. For example in case of a-Si the Sr is quite poor in the range of short wavelengths, because of the poor ability to collect the charge carriers in the p-layer [14]. In the case of long wavelengths the Sr may be very poor when the i-layer is not thick enough compared to its optical path and thus, the absorption of light is poor [14]. In general the Sr is influenced by doping as well as impurities, as they influence the material structure. As a consequence e.g.

[4]The conversion between band-gap energy and corresponding wavelength can be done with the formular $E = \frac{hc}{\lambda}$ [14].

the band structure, but also light absorption, carrier life-time and recombination processes are influenced [14].

Talking about the influence of the properties of different semiconductor layers on the Sr, those layers have most impact within only a certain wavelength range. The p-layer (i.e. the emitter) has only influence on the Sr in short wavelengths range [21]. Within the range of visible light the embedding material, i.e. the TCO, has its influence on the spectral response [21]. And finally in the range of long wavelengths, the n-layer is mainly influencing the Sr [21]. Due to stronger reflection of very short or very long wavelengths the QE is further and much more reduced in that wavelengths ranges than in the remaining wavelengths range [22]. Since one could go deeply into details about properties of different materials and their influence and it could easily fill books, there will be no further discussion within this work.

2.4. Introduction to existing Sr-measurement systems

In this chapter different existing Sr-measurement systems, capable of PVs-modules and devices of similar size, will be described. Since those devices are of economic importance the published information is very limited. Therefore only key details can be presented. If available also issues, advantages and limitations are briefly presented.

In [21] a Sr-measurement system, with the purpose to map the spatial uniformity of the Sr of thin film modules, is described. The basic concept is similar to the state-of-art systems for measurement of solar cells. The light source is a halogen lamp. Then this light is being filtered with different filters in a filter-wheel, to narrow down the bandwidth. For further reduction of the bandwidth filtered light passes through a monochromator. However, the final bandwidth of the monochromatic light is not published. The monochromatic light is chopped to distinguish between the coloured bias light and the monochromatic light for Sr-measurement. Then the light is brought on the device under test via thin fiber. The produced monochromatic spot has a diameter of $3\ \mathrm{mm}$. That light spot can be moved across the module surface to spatially map the Sr of the PV-device. The current signal is amplified and measured with a lock-in amplifier. As a conclusion about this system the research group states a reproducibility of the measured Sr within less than $\pm 1\ \%$. However, as a disadvantage the group found, that the measured Sr depends strongly on the distance between the light spot and the contact.

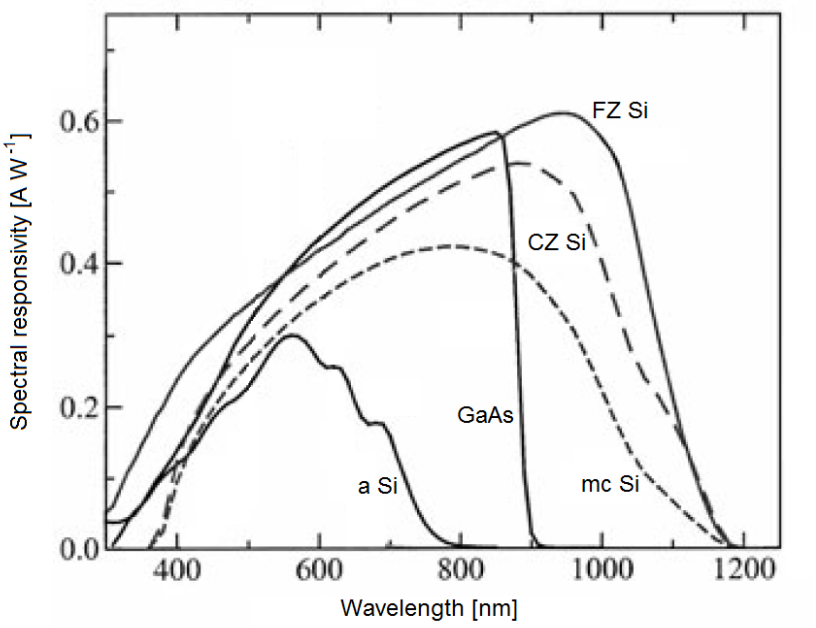

(a) from left to right: amorphous silicon, GaAs, multi crystalline silicon, mono-crystalline (Czochralsky) silicon, float-zone silicon. (after [10])

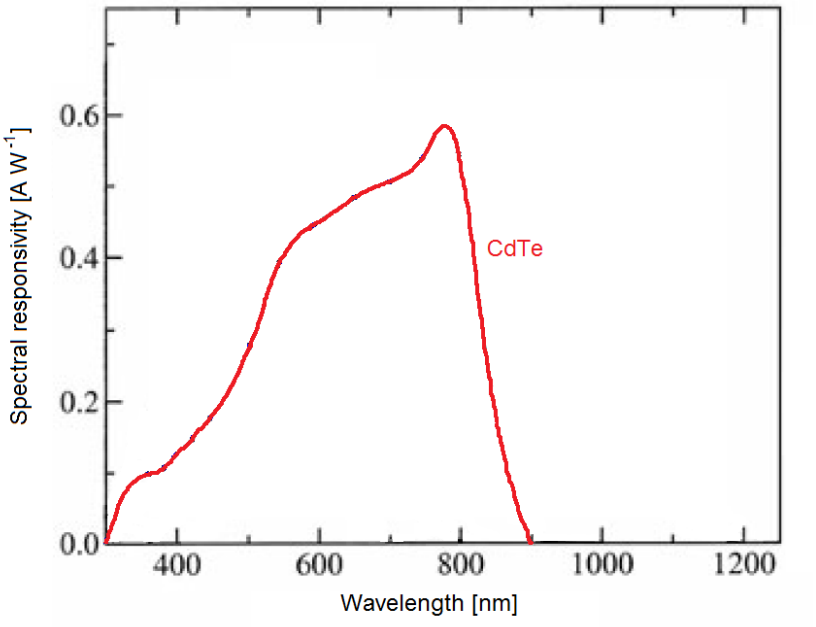

(b) CdTe, see figure 4.4. (after [7])

Figure 2.6.: Comparison of the spectral response of different solar cell types.

Another system, similar to the one finalized through this work, is described in [23]. The light source are two Xe lamps used in a Pasan IIIb. The light source is pulsed with a pulse duration of 10 ms. Then the light is filtered by a arrangement of interference bandpass filters with a band width of 25 nm. The filters range from 360 to 1170 nm. In the case of this system the complete PV-module is illuminated. The system was validated by comparison of the measurement results with measurements of the Physikalisch-Technische Bundesanstalt Braunschweig. It is said, that this system can be used for the measurement of single junction devices without bias light, since the intensity of the monochromatic light is sufficient enough. For the measurement of multi-junction devices appropriate coloured bias light is required. Details about the measurement accuracy are not published.

A different approach for the Sr-measurement is addressed in [24]: the use of Light Emitting Diodes (LEDs) for illumination. In that work once only four and once six different LEDs colours have been used in order to create a small prototype. In that work two issues arise. On one hand there is the issue of spatial homogeneity of the light intensity. The homogeneity depends on the area illuminated by one single LED and on the distance of the LED-panel to the PVs-device. After optimisation the spatial homogeneity became as low as 3 %. On the other hand, there is the difficulty to achieve irradiation with sufficient intensity. This problem is reported to be unsolved until time of publication. The irradiation intensity was too low for a proper Sr-measurement of a solar cell.

Chapter 3.

Measurement Concepts

The basic concept and example of measuring the Sr is shown in figure 2.5 on page 24. With any kind of monochromator one filters light from a light source. This light of finite bandwidth illuminates the sample cell or module and a reference cell. With the reference cell of known Sr the incident irradiance per unit area is determined. At the same time as the sample cell or module is illuminated its output current is measured. The Sr is then basically calculated using the equation (2.17) on page 22.

However, in order to find a suitable concept several constraints, due to technical limitations, budget and normative regulations have to be considered. Since it is desired to integrate the Sr-measurement system into an existing system for measuring the I-V-curve of PV-modules or -cells with a pulsed flash-light, one has to consider the dimensions of the existing measurement system as a constraint. One raising question was if the existing pulsed flash-light is used (if possible) or if new light sources have to be installed. Furthermore the most important technical limitation is that the whole area of commercial PV-modules has to be illuminated with (quasi-)monochromatic light.

That this kind system is limited by international standards is generally not a requirement. Since it was planned to use the Sr-measurement system, besides for measurements out of curiosity and for research purposes, even for rating of PV-modules according to international standards those have to be considered in the concept, too. Besides the standards for measurement devices used in the system, e.g. ampere meter, the most important one is the IEC 60904. It applies to everything concerning PV-devices. In the present work about the measurement of Sr specifically the part 8 is applicable, thus it is the standard IEC 60904-8 [2] with the title “Photovoltaic devices - Part 8: Measurement of spectral response of a photovoltaic (PV) device”. The key restrictions are the followings: [2]

- bandwidth of each filter $\delta\lambda \leq 50$ nm
- measurement interval: at least every 50 nm or smaller [1]
- side-bands of transmission spectra ≤ 0.2 %
- spatial uniformity of irradiance at the module (i.e. test) plane ± 2 %[2]

Furthermore it is necessary to use bias light unless it is proven that the measured Sr is not changing significantly compared to the case of not using it [2]. This applies mostly to cells with a linear dependence. Special care has to be taken with modules whose cells show non-linear behaviour in the irradiance/output-current relation. Those have to be measured at a bias voltage [20].

In addition the system has to be rated according to feasibility, flexibility and capability. The criteria are meant and can be understood as follows: The feasibility of a system is rated according to the question if it is possible at all, projecting the light from a light source on the PV module size, how easy one can get the necessary components, the amount of components or material necessary and how easy it can be designed and built whilst not losing its functionality. The rating according to its flexibility refers to the system-capability of measuring Sr for different cell technologies, i.e. if it is capable of only measuring Sr of modules made of common Si-cells or even measuring thin-film- and/or multi-junction cells. The capability of a system is rated better when one system is less complex and/or less difficult to be set up whilst keeping same flexibility and feasibility as the other similar systems. A criterion additional to the above mentioned ones is the cost of the system. A comparison of different possible systems with their evaluation according to these criteria is found below in the chapter 3.1.

3.1. Concepts in Discussion

Several different ideas have been developed or thought of for the purpose of realizing a measurement system for Spectral Response (Sr) of PV-modules. The ideas concerned questions as how to get monochromatic light from an existing white light source or if there are already quasi-monochromatic light sources available? Further more how to focus and later diffuse light by an optical system in case it is necessary? Is it possible to illuminate an area of

[1] The intervals have to cover the complete non-negligible range of the modules Sr, to give a complete Sr-picture for the module type in test.

[2] The value of spatial uniformity is not specified by the 2nd edition of IEC 60904-8, but is mentioned in a committee draft for the 3rd edition.

around $1.5\ \mathrm{m} \times 2.0\ \mathrm{m}$ or larger or actually how to illuminate this large area? For all questions it was necessary to find a solution that is usable for almost all available types of PV-modules also concerning thin-film-modules. In the following only the most promising concepts are introduced for discussion.

3.1.1. Optical filter foils

The concept of using optical filter foils for cutting off the spectrum except a small bandwidth is very simple.

Since most of the necessary information about optical filter foils is available for filters manufactured by *LEE Filters* and they are the most famous company for these filters. All assessment of this possible method is done using their product range and product data.

Advantages:

- Measurement system can be built easily.
- Filters and component can be purchased very easy.
- Low costs compared to glass filters.
- Available as foils with larger size (compared to glass filters) $\longrightarrow$ possibility to illuminate large areas.
- Possibility to upgrade the system for multi-junction & thin-film modules easily.

Disadvantages:

- Thermal degradation of filter foils $\longrightarrow$ only usable with pulsed light.
- Only low transmission for the filters with acceptable bandwidth: $\lesssim 40\ \%$ or $\sim 10\ \%$.
- Bandwidths mostly $\gtrsim 50\ \mathrm{nm}$ and only very few filters with acceptable bandwidth of $\lesssim 50\ \mathrm{nm}$.
- Increasing transmission at all filters for wavelengths of $800\ \mathrm{nm}$ and greater - IR transmissive tail (see fig. 3.1: increasing transmission at $750\ \mathrm{nm}$ and onwards)
- No bandpass filters at lower wavelengths.

Unfortunately, as short pass filters are not available a combination with the variety of long pass filters is not possible. Therefore and because of the disadvantages a system based on filter foils is not feasible and possible costs have not been estimated. However, filter foils with the characteristics of a long pass filter can still be considered for coloured light BIAS; especially for the use with multi-junction or thin-film modules. More information on this possibility will be discussed later in chapter 3.2.3 on page 52.

Note: All information on available filters have been gathered from the Spectral Charts published by LEE Filters on their web page [25]. Detailed spectral data was provided on request and is unpublished. The latter is the source for graph 3.1

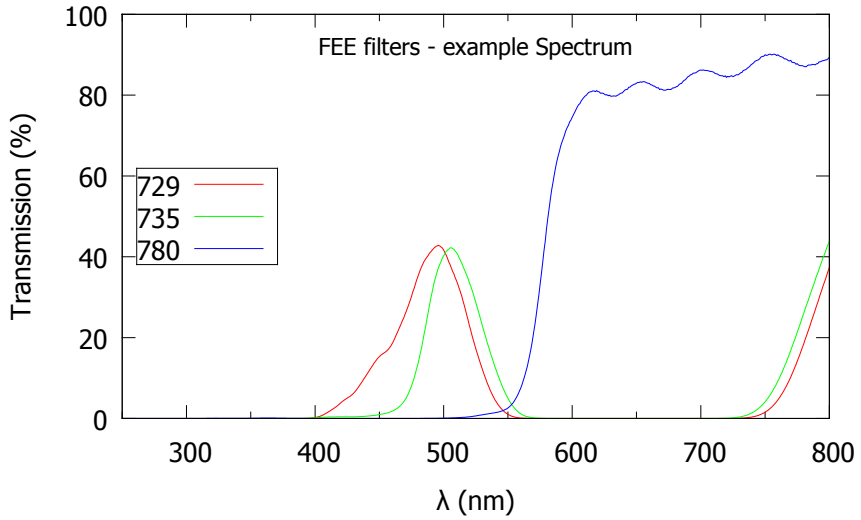

Figure 3.1.: Transmission spectrum of three example filter foils by LEE Filters: Filters No. 729 and 735 are bandpass of best quality (according to the needs for this work). Filter No. 780 is an example of the various long pass filters.

3.1.2. LED field for quasi-monochromatic illumination

A contrary concept is the use of an LED-illumination field. Instead of filtering a white light source which results in quite low irradiation on the module plane a LED-field is a reasonable idea. The LED-field is supposed to consist various different LEDs with different peak-wavelengths but only a narrow emission bandwidth as required by the normative regulations. The number of different LEDs used only depends on the desired accuracy for the Sr-measurement curve and has a lower limit given by the standard [2], i.e. at least every $50\ \mathrm{nm}$. LEDs of the same spectrum have to be distributed equally on the LED-field, thus

giving a homogeneous illumination along the PV-module plane as required by the standard [2]. For reaching a sufficient irradiation on the PV-module the distance between that and the LED-field is roughly estimated to be around $10 - 20$ cm. However, this distance can be easily adjusted thus having the possibility to change the irradiation per square-meter if required. As a requirement it is obvious that the LEDs of different spectra have to be switched on independent of each other to reach quasi-monochromatic illumination. This on the other hand give the possibility to turn on several LEDs with different spectra at the same time to achieve a BIAS light of a arbitrary spectrum. The whole LED-field including the PV-module to be measured has to be completely sealed off from outside-light.

Advantages:

- The LED-field can be built in smaller LED-units (e.g. PV-cell size) , thus the LED-field is expandable and easy to maintain (only defect units have to be replaced).
- As the size is arbitrary it is easy to illuminate large areas.
- LEDs are existing with small $\Delta\lambda$ (e.g. ~ 10, 15 or 20 nm).
- Such a system is capable of multi-junction and thin-film PV-modules.
- No separate BIAS light is needed. It can be turned on by a selection of LEDs of different spectra to create the desired BIAS.

Disadvantages:

- Relatively hight heat dissipation of LEDs ($\sim 65 - 80$ % of electrical power input[3]): cooling is necessary, but also doable.
- LEDs have mostly quite low irradiation power: high density of LED necessary.
- No LEDS with λ above 1200 nm and a lack of wavelengths between 730 nm and 850 nm.
- The workload is expected to be high if the system has to be built on our own.
- Expected price of the components: $\sim$100000 € (one of the most expensive systems possible).

Finally this idea was not finalised due to the limited availability of LEDs in the wavelength range between 300 and 1300 nm, the expected workload for building up such a system and even the height of the expected costs.

[3] value named during a phone call with technical support of NICHIA CORPORATION in Nürnberg

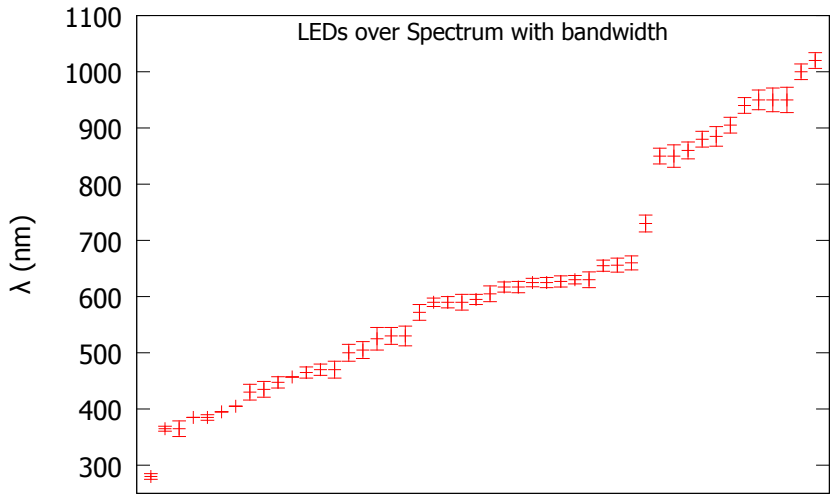

Figure 3.2.: List of LEDs found at different companies. Marks at centre wavelengths with error bars representing the bandwidth.

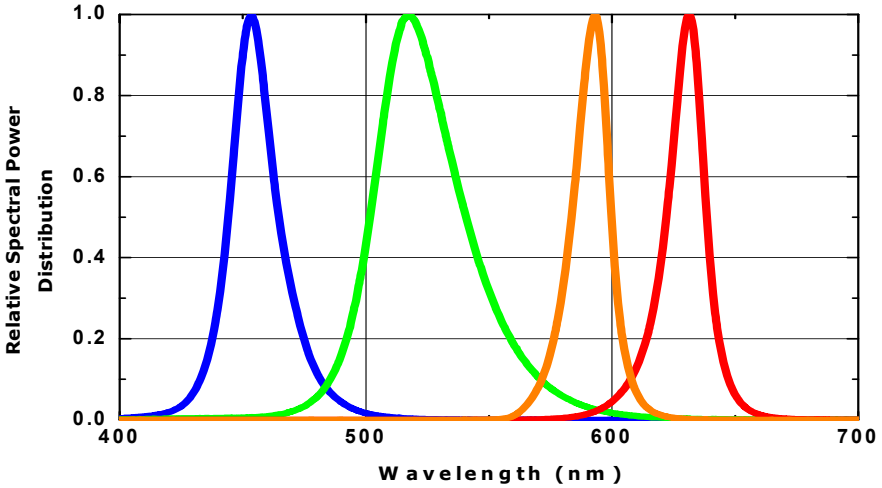

Figure 3.3.: Example spectrum of some LEDs. Colours from left: Red, Amber, Green, Blue (Royal Blue). [3]

3.1.3. Optical Bandpass filters

The use of optical bandpass filters based on interference is another possible solution. The big advantage is the existence of such filters throughout the whole spectrum and within the specifications given by the normative standard for Sr-measurement. The concept of this system is to place on one side the PV-module, on the opposite side the light source and to put the different bandpass filters as required in between the two. The distance of each of the three items has to be figured out in such a way that the light beam going through the filters

covers the whole PV-module.

Advantages:

- Relatively easy to be built.
- Components can be purchased very easy.
- Costs for this system is very reasonable with $\lesssim$40000 €.
- The system can be added to the existing measurement component (no separate measurement system or space needed).
- The system can be upgraded for capability to measure all different types[4] of PV-modules.
- The required filters are available with a bandwidth of $20\ \mathrm{nm}$ at peak wavelengths in steps of $50\ \mathrm{nm}$ throughout the whole required spectrum.

Disadvantages:

- Size of the bandpass filters is only available as $5 \times 5\ \mathrm{cm}$, therefore patches of filters with the same peak wavelength are needed.
- BIAS light has to be built in addition to the existing light source.
- It is difficult/impossible to build the system for very large/arbitrary PV-module sizes.
- The peak-wavelength of interference bandpass filters has a dependence on the angle of the incident light.

As this system seemed to be the most feasible while being capable of measuring different module types (at least under further extension of the system), relatively easy to be built and quite inexpensive it was chosen to be built up as an extension of the existing I-V-measurement system for PV-modules. The serious disadvantage of the light-incidence-angle dependence of the peak-wavelength is accepted in this case and it's impact will need investigation. All details on this system will be explained and discussed later in chapter 3.2.

[4] all types known up to date, i.e. Si-based single-junction, multi-junction and thin-film PV-modules

3.1.4. Optical Bandstop filters

Using bandstop (Notch-) filters in stead of bandpass filters is another possibility. Though the concept is the same in both cases which is leading to almost the same advantages and disadvantages. From construction point of view it is the same in both cases.

Contrary to the use of bandpass filters there is one advantage that arises from the transmission characteristics of bandstop filters. As one can see in transmission spectrum of an example Notch-filter by Edmund Optics Inc. (see figure 3.4) the transmission of light is around $90\ \%$ over the whole spectrum except a small band of $\sim 25\ \mathrm{nm}$ where the transmission is close to zero (in the example the filter has an optical density (OD) of ~ 6 (that means a transmission of $\lesssim 10^{-6}\ \%$). Therefore bias light is already given by default which would simplify the system by that one component more. Another advantage due to that spectrum characteristics is that the PV-modules can be measured under usual load. Furthermore the measured Current signal is very high (around the maximum possible/expected current under load at the given light irradiance). Because of this it can be expected that the noise measured is very low or negligible compared to the signal drop caused by cutting out a small part of the spectrum. Thus the error for the measurement can be expected to be smaller than for the use of bandpass filters.

However, since the price is around triple or even more compared to bandpass filters this system was decided to be not realised.

3.2. Chosen Concept

As it was mentioned in chapter 3.1.3 due to the simplicity and relatively low costs compared to the high capability it was decided to realise a concept with band pass filters. In this chapter the concept as it was finally designed and implemented is described in detail. It will be described how it is working and how it will be used in the implemented state, and the potential of the created system will be described as there are still small extensions missing for its full capability.

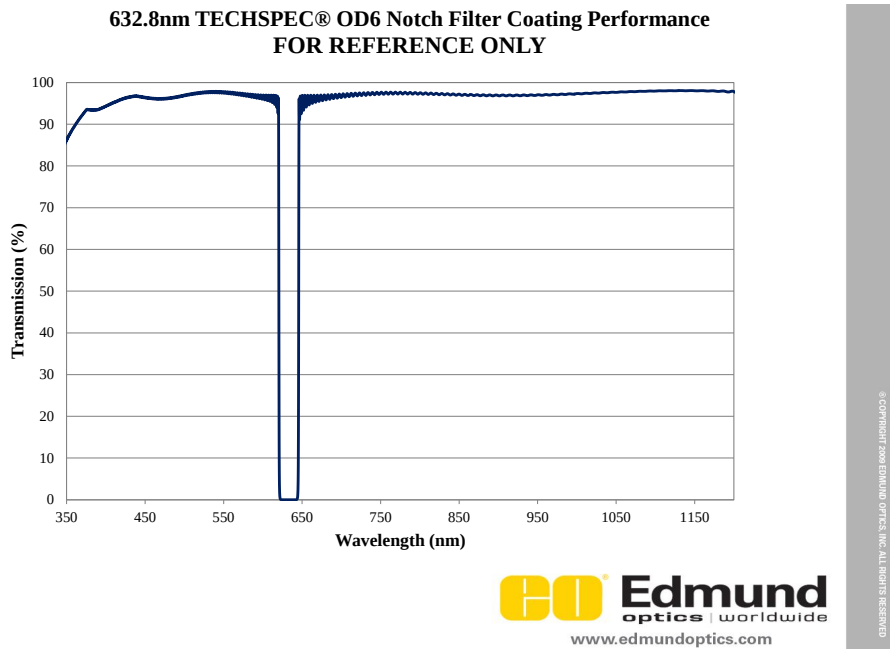

Figure 3.4.: Example spectrum of a Notch-filter by Edmund Optics Inc. with OD 6 for the band stop. Peak wavelength $\lambda_0 = 632.8$ nm, bandwidth $\Delta\lambda = 25$ nm. [4]

3.2.1. Description

The construction for the bandpass filters is an “add-on” to the existing measurement system for the I-V-characteristics of PV-modules. The original system uses a flash lamp (i.e. flashing in short irradiance pulses) which in the new construction (in Sr-measurement mode) is used for the illumination through the bandpass filters. In this case the complete system can be used for both, either I-V-characteristics or Spectral Response measurements. The “add-on” construction for the filters holds three carriages with all together 20 slots for different filters and an additional carriage which works an aperture to block light from around the filters. The carriages are electronically driven to ensure easy usage. For the Sr measurement the filters will be moved with those carriages inside the lamp housing. For each wavelength step to be measured the test-module will be illuminated by one flash with the corresponding filter inside.

Original I-V-Measurement system

The original I-V-measurement system which was extended through this project consists of a housing (dark room), the lamp (plus necessary equipment) and the measurement equip-

ment.

The housing is a tower with $2.8\ \mathrm{m}$ in width, $2.5\ \mathrm{m}$ in depth and $\sim 8\ \mathrm{m}$ in height. The inside is absolutely insulated from the outside-light. Inside this tower at the top is a construction holding the lamp for flash-illumination. At the bottom of the housing (at around $1\ \mathrm{m}$ above the floor) is the test-plane level where the PV-modules or -cells and the reference device can be placed. The lamp for flash-illuminating the modules and the necessary electronic equipment

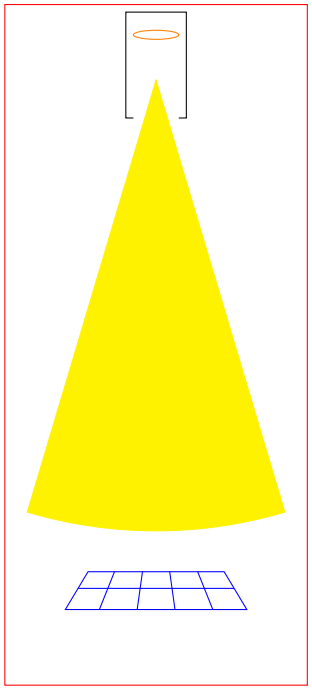

Figure 3.5.: Sketch of the housing (red) for the illumination system with lamp (top; lamp: orange, lamp-housing: black) and test module (bottom; blue).

is a PSS 30 by BERGER Lichttechnik GmbH & Co. KG (in the following called “Berger”). The spectrum of the lamp is certified as AM 1.5 with spatial homogeneity and temporal stability of Class A [26]. According to the specification the lamp achieves an irradiation of $1000\ \frac{\mathrm{W}}{\mathrm{m}^2}$ [26]. The flash produced by this lamp lasts for a duration of $13\ \mathrm{ms}$ of which $10\ \mathrm{ms}$ can be used to actually perform a measurement under stable conditions [26].

For the measurement of the I-V-characteristics measurement-equipment by Berger Lichttechnik and Pasan is used. Both measure simultaneous the voltage and the current of the reference cell whilst sweeping through a given voltage range for the PV-module in test to measure the I-V-characteristics. However, for use at low current output the system by Berger Lichttechnik is not recommended and the one by Pasan is at the lower limit to still measure the current output.

Filter-System

Since bandpass filters have been chosen to produce quasi monochromatic light the actual work phase of building or designing was to create a system that can hold the filters and that can move the filters inside the lamp. Initially the filters have been thought to range from $300\ \mathrm{nm}$ to $1300\ \mathrm{nm}$ with wavelength steps of maximum $50\ \mathrm{nm}$ (see normative regulation on page 30). The range is decided to cover the spectrum where the Sr of all different PV-modules and especially the one of mono c-Si-modules is non-negligible plus some buffer. The final decision was to have 20 Filters that actually cover the spectrum from $300\ \mathrm{nm}$ until $1250\ \mathrm{nm}$ which is not a problem at all in respect to the necessary range. Because of availability of filters in this range and in order to have enough current output without bias light as well as lower errors as with wide bandwidths the decision fell on filters with a bandwidth of $20\ \mathrm{nm}$.

Research at bandpass filter producers and sellers made clear that filters of suitable quality are only available at a maximum size of $50 \times 50\ \mathrm{mm}^2$ (squared). In general bigger custom sizes are available on request, however, only for a much higher price and of less quality since it is hard to achieve a sufficient spacial homogeneity of the interference layers on larger substrates. As a consequence the filters need to be put together in order to cover larger areas. However, this also leads to other problems affecting spatial homogeneity of the irradiation on module plane (e.g shading), difficulty to even assemble the filters of same wavelength together and the slightly different spectra of each filter (shifted peak wavelength, bandwidth, transmission intensity over the spectrum).

By doing a rough and geometrical estimation the necessary filter-area has been derived. Assuming a distance of $4.3\ \mathrm{m}$ between the lamp itself and the module-plane and only considering direct illumination (no diffuse light and not considering the opposite side as source) from the lamp with a outer radius of $\sim 8\ \mathrm{cm}$ (see the lamp in fig. 3.7) it is suggested to use a total filter area of $15 \times 10\ \mathrm{cm}^2$. As one can see in figure 3.6 with a filter-area of $10 \times 10\ \mathrm{cm}^2$, i.e. 2×2 filters, the illuminated area reaches approximately an area of $1.1 \times 1.1\ \mathrm{m}^2$ which is too small to illuminate a usual PV-module. Enlarging the filter-area to 3×3 filters, thus $15 \times 15\ \mathrm{cm}^2$ the illuminated area reaches $3.9 \times 3.9\ \mathrm{m}^2$. In order to reduce the costs for filters it was decided to use an array of only $3 \times 2 = 6$ filters, thus $15 \times 10\ \mathrm{cm}^2$, which results in an illuminated area of around $3.9 \times 1.1\ \mathrm{m}^2$. This is enough to measure at least small or medium size PV-modules. Measuring the homogeneity of the irradiance using a moulding tool, i.e. an aperture with a rectangular hole of $16 \times 11\ \mathrm{cm}^2$, showed that an area of around $1.6 \times 1.0\ \mathrm{m}^2$

has a irradiance homogeneity of $+2/-3\ \%$ [5]. The more tolerant homogeneity is accepted in this case to reach a usable area on which modules can be measured for reasons of research and comparison despite not being a measurement according to the normative regulations. In addition a different final homogeneity is expected as the frame holding the filters has a different effect on the homogeneity then a rectangular hole. In this case trial-and-error is the method followed to finalise this prototype.

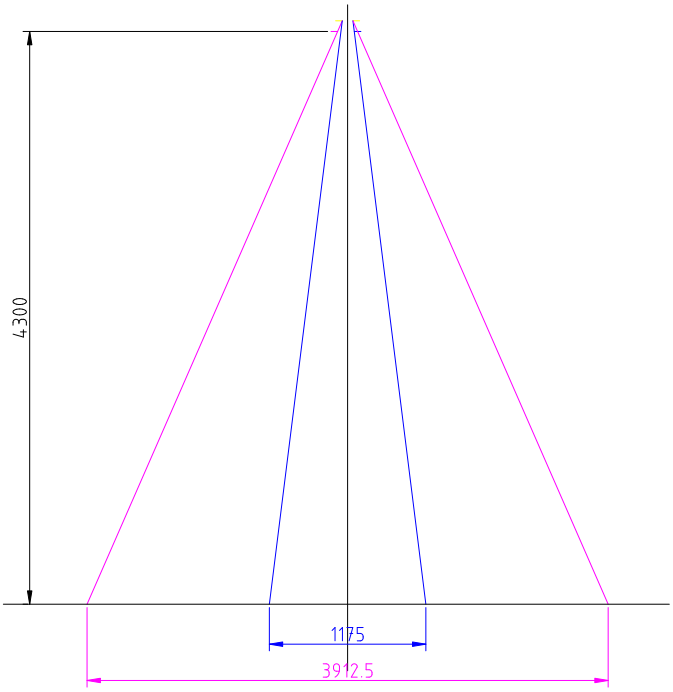

Figure 3.6.: Geometric estimation of filter-area (units in mm). Yellow: markings for the lamp dimension, $8\ \mathrm{cm}$ are marked by the gap between the inner line-endpoints. Purple: direct beam and dimension of filter-area for $15 \times 15\ \mathrm{cm}^2$ filter-size; Blue: direct beam and dimension of filter-area for $10 \times 10\ \mathrm{cm}^2$ filter-size (inner line-endpoints of horizontal lines mark the filter-area-dimensions, diagonal lines mark the beam)

The filters of same wavelength are assembled together with a frame made of glass-fiber-circuitboard. This filter-holder consists of a layer below the filters (i.e. the filters are put on this frame) and a layer that is put on top of the filters to prevent them of falling out of the structure and keeping them in place (see figures 3.8, 3.9). The top-frame is designed with cross-like ribs, so that light can not pass to the filters at certain areas. This is necessary as

[5] note: homogeneity according to the normative regulations is required to be within $\pm 2\ \%$.

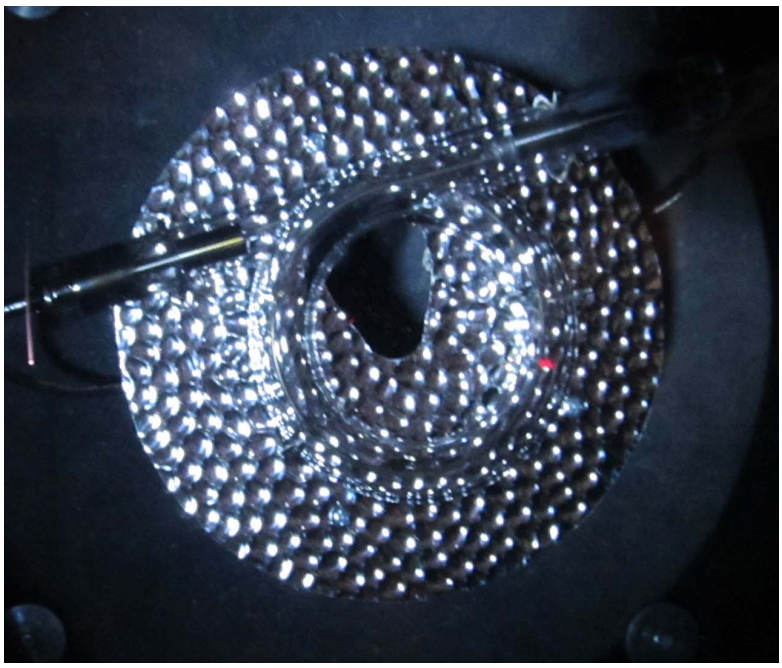

Figure 3.7.: Picture of the halogen lamp used. Shape: torus; Diameter: ~ 8 cm.

the filters have a margin of 1.5 mm (from the outer edge) where they are not coated with interference layers. Thus, light could pass through the filters without being blocked in this area. However, since light exits the filters filtered this cross-like rib is not necessary for the bottom-frame. Further more it was decided for only one rib along the filter-holder so that light exiting non-perpendicular to the surface is not being absorbed by too many ribs, i.e. being lost irradiance for the measurement. It is obvious that this rib is necessary to carry the filters, otherwise the two out of six filters in the middle position are in danger to fall out of the construction. (see figure 3.8) As one can see in figure 3.9 there is a layer of foam plastic material put along the filter-carriage along two sides of the filters and between the frames made of glass-fiber-circuitboard. That is used as material with variable thickness. Its purpose is to ensure a variable thickness of the gap between the two frames for the filter-holder, thus, the filters can be fixed in between without having a remaining gap to vibrate vertically when the filter-carriage is being moved. With those frames the filters of same peak wavelength are not only put together, but also assembled and mounted on the filter-carriages. Such a filter-carriage without mounted filters can be seen in figure 3.10 and with two filters mounted and fully assembled in the system in figure 3.11.

The filter-carriages are put on rails on which they can be moved from outside the lamp housing into the housing with the required and used filters exactly below ($\sim 3 - 6$ cm) the lamp. The view of carriages in a arbitrary position inside the lamp-housing can be seen in figure

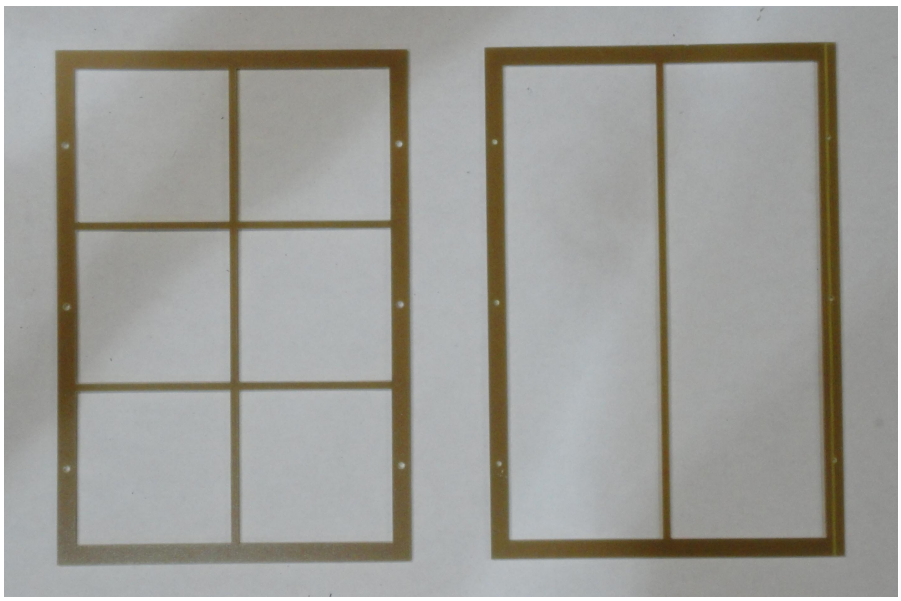

Figure 3.8.: Unmounted frames for filter-holder. left: top-frame with cross-like ribs, right: bottom-frame with one rib along the longer side.

3.12. The motion is done my stepper-motors that drive driving-belts which are connected to the carriage-ends. Since the driving-belt would be inside the light beam, the effected part of the driving-belt is replaced by a thin rope to reduce shadowing. Due to the very small diameter of the rope, potential shadowing might be compensated by diffraction of the light. The timing-belt construction required additional components to be developed: One is a stretcher to keep the timing-belt under constant tension. The second is a connection between one end of the timing-belt and one end of the thin rope. This connection also serves as a possibility to adjust the total length of the timing-belt (including the rope) to compensate the loss of tension with time. However, those two components developed for this work will not be described further in here. Altogether there are three carriages, two with seven and one with six filter-positions respectively. Those can be moved inside the lamp independently. In addition there is an aperture (as well built as a carriage) that is moved inside the lamp-housing when filters are moved inside. The purpose of the aperture is to block light that could pass by the filter-carriages since those are not as wide as the diameter of the aperture inside the lamp-housing (which is $35\ \mathrm{cm}$). The configuration of all 4 carriages and how they are arranged inside the lamp-housing can be seen in the construction-plan in figure 3.13. Therefore the width of the aperture-carriage was planned to be $39\ \mathrm{cm}$ (arbitrary value in compliance with the dimensions of the lamp-housing and its components, i.e. an overlap on both sides by $2\ \mathrm{cm}$, thus eliminating as much diffuse light as possible). For this the lamp-housing would have been to be adapted so the carriage fits inside and passes through. Unfortunately, the necessary

changes turned out to be not doable. Therefore the width of the aperture-carriage needed to be reduced to $29.9\ \mathrm{cm}$ to fit through the housing. This obviously leads to a unblocked gap where white light is able to pass through and reach to the module-test plane.

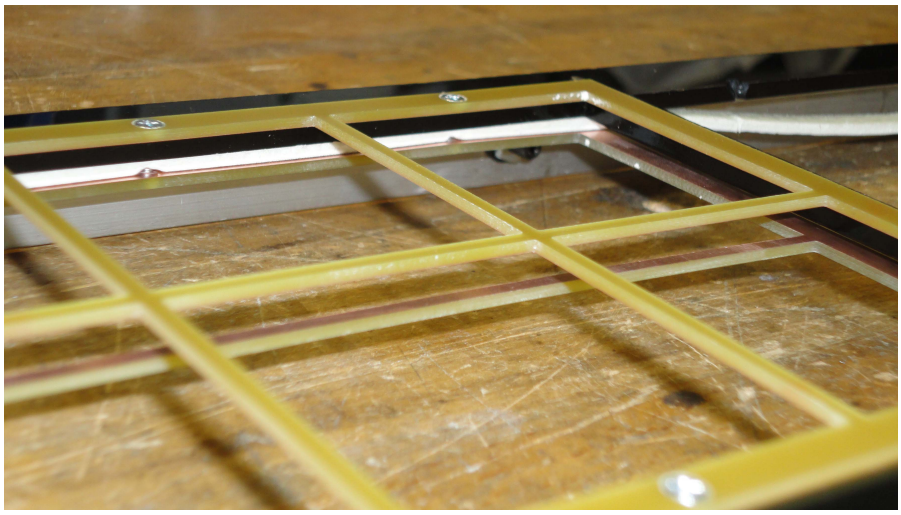

Figure 3.9.: Mounted filter-holder without filters at a filter-carriage. On the upper part of the picture visible: layered structure with top-frame, carriage-frame, foam plastic material, bottom-frame.

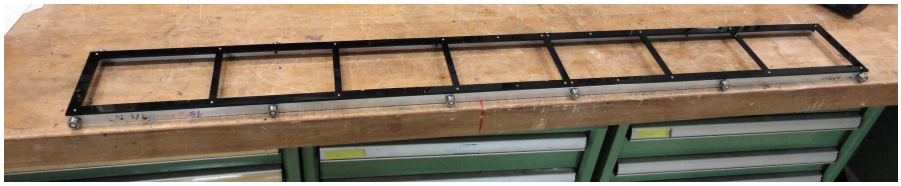

Figure 3.10.: Clean filter-carriage without any mounting frames.

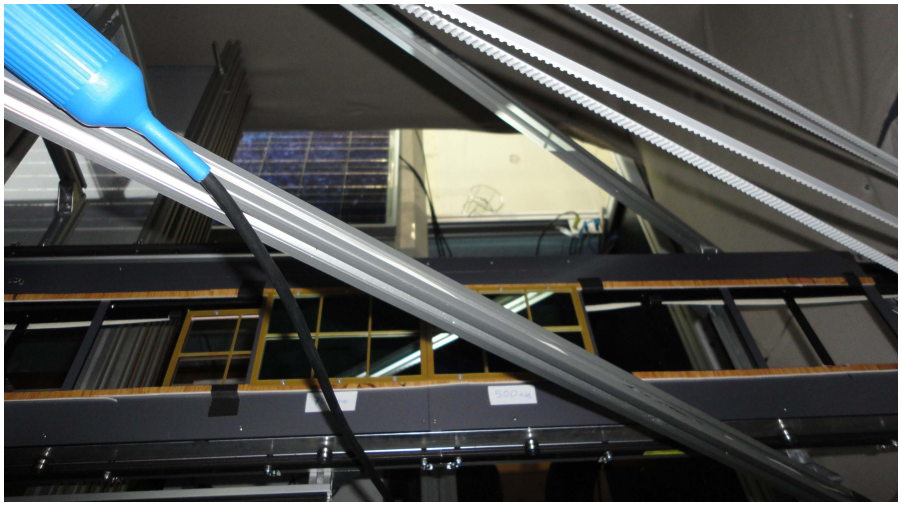

Figure 3.11.: Filter-carriage assembled inside the system, ready-to-use.

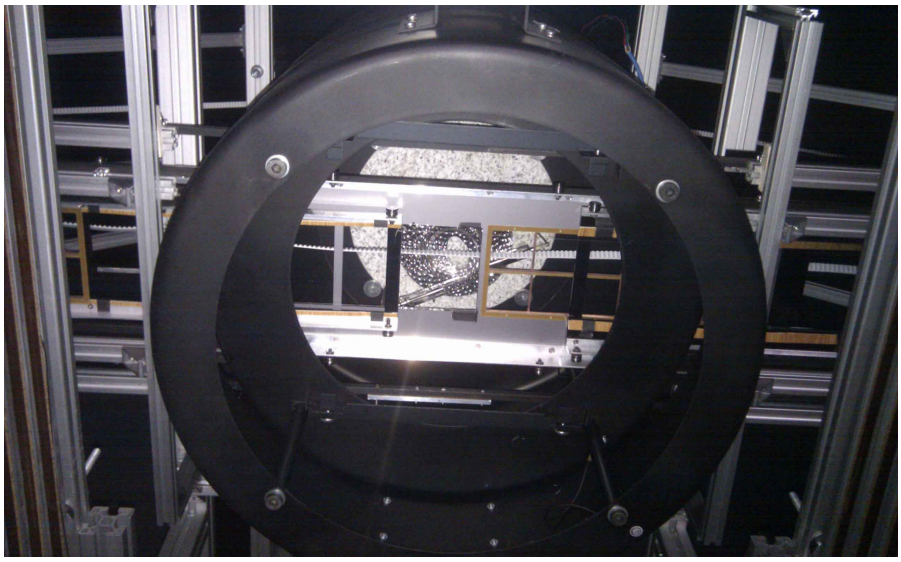

Figure 3.12.: Filter-carriage assembled inside the system, view of inside the lamp-housing.

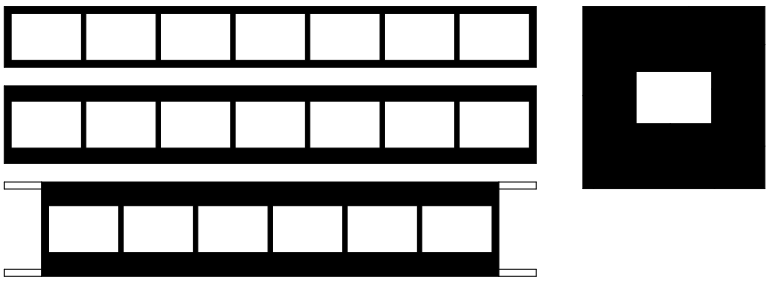

(a) Top-view to all carriages: left side (from top): carriage 1, 2, 3; right side: aperture-carriage.

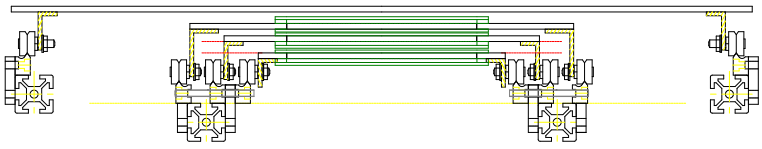

(b) View of the arrangement of the carriages relative to each other from the left side of the system: (from top) aperture, filter-carriage 3, 2, 1.

Figure 3.13.: Configuration of all 4 carriages and arrangement inside the lamp-housing (construction-drawings).

Electronics

After describing and explaining the main assembly of the system – the optical filter-assembly – this chapter will give a short description of the required side-assembly – the electronics. In this case it will be referred to the electronics required to power/move the filter-carriages and the aperture-carriage, but not the actual measurement equipment, e.g. Volt-/Ampere-meter.

Since the carriages perform a linear motion on straight rails and the filters have to be aligned exactly in the centre below the flash lamp, i.e. the bulb, for usage exact positioning is required. Thus one has a defined "home"-position, i.e. defined at position $\mathrm{x} = 0\ \mathrm{mm}$, and a position of the carriage when one filter, e.g. A3, is centred exactly below the bulb. This can be for example after moving the carriage for $\mathrm{x} = 745\ \mathrm{mm}$ [6]. In fact the position of each carriage is well defined for every single filter-position to be set.[7] Therefore the best solution to ensure exact positioning is using stepper-motors, as already mentioned in the previous chapter (see application in printers). An advantage is that hardware for stepper-motors is available and easy to be purchased since it is used for 3D-printers (non-commercial devices). The software for those is available as open-source. To reduce amount of work those are the best option available as it can be used after only few adaptations, i.e. the 3 printer axis control the motors for the 3 filter-carriages and the fourth motor originally used for printer-material feed can be used to drive the aperture-carriage. More details on the hardware will follow in one of the next paragraphs.

In the following some details on the components will be given: The stepper-motors used are of the type QSH4218-51-10-049 by Trinamic. The key parameters are:

Rated Voltage	V	5.0
Rated Phase Current	A	1.0
Phase Inductance (typ.)	mH	8.0
Holding Torque (typ.)	Ncm	49

Amongst those parameters the holding torque is the most important one to decide for a certain model. It tells which torque it can still hold when not moving without losing steps.

[6] This value for the position is arbitrary and only serves as an example.

[7] It has to be mentioned that these values change slowly by time and have to be reconfigured. This is because the carriages are driven by the motors via a driving-belt (A portion of the driving-belt length is replaced by a very thin rope where the driving-belt would be inside the light-beam and thus shadow a portion of the beam. The thin rope is thin enough to minimize the influence to be literally un-measurable.) which will expand under the tension.

Connected to this as well is the torque which is depending on the speed. The decision which model to take is quite difficult as it requires a lot of experience in addition to the physics parameters of the set-up. Besides, it takes too much time to calculate physics of the set-up in order to make the decision. Therefore this one was suggested by experienced users of stepper-motors. However, the general approach for a decision is relatively easy to explain: Addressing the measurement system to be discussed here one can say that the holding torque could be low as the movement is horizontally only and no weight has to be lifted and kept at a certain hight. On the other hand considering an reasonable acceleration of a carriage a higher torque might be desired. Looking at our case this motor has more than enough torque: One carriage with seven slots of filters has around $2.100\ \mathrm{kg}$. The weight of the carriage itself might be another half a kilogram. Considering an acceleration of $1\ \frac{\mathrm{m}}{\mathrm{s}^2}$ which is extremely high and the force pulled by a gear with $3\ \mathrm{cm}$ diameter we reach a necessary maximum torque of $0.075\ \mathrm{Nm}$. Thus, for acceleration even less than $10\ \%$ of the holding torque might be required. In practice this turned out to be still necessary as the rails are not exactly straight and in some cases the wheels have to be pulled over small gaps. Especially in those cases it is important to not loose steps as the position would be wrong.

The hardware used to control and power the stepper-motors is again a component used for amateur 3D-printers (as already mentioned a few paragraphs before). The circuit board keeping the electronics specifically for running a 3D-printer is the so called “Ramps 1.3” (short RAMPS) which is open hardware. This circuit board requires the Arduino Mega 2560 as a controller board. The RAMPS supports all necessary features, i.e. powering and controlling the stepper motors (altogether four motors), end-stops, and a fan to cool the components especially the motor-drivers. The end-stops used are optical end-stops, i.e. photo-electric guards, which define the “home” position with $x = 0\ \mathrm{mm}$. Altogether RAMPS has already a support for six end-stops of which two each are minimum and maximum stops for the three axis x, y, z. However, only the three minimum end-stops are used, plus for the fourth carriage another end-stop was connected to free customizable pins. The necessary adjustment has to be done within the software (i.e. the firmware). The maximum end-stops are kept free, instead the endpoint for the carriages is defined inside the software. The whole controller unit can be seen in figure 3.14 and an end-stop in action in figure 3.15. Again, the advantage of this decision is that free software can be used with only very small adjustments. Controlling the carriages is then done via the open source software “printrun master” (again used for 3D-printers). This software has a easy to use GUI with customizable buttons that can be programmed for e.g. one for each filter-position.

The communication between the computer (via Printrun Master) and the controller board is done via serial communication. In general the communication between software and controller board is supposed to be done via USB-connection. But serial communication was suggested to be more EMC-prove[8]. Serial communication is also possible for the controller board. For this purpose Transmit and receive pins are existing. To cover the distance of around $10\ \mathrm{m}$ a shielded network-cable of CAT6 is used for the serial-communication. The shielding is necessary as the cable to supply the flash lamp with electricity is close by and high currents are expected during each flash. This is a measure to make the communication EMC. A USB-to-serial converter is plugged in at the computers USB-port. The serial converter is from FTDI and has the type number TTL-232R-5V-WE. However, during tests the connection between computer and Arduino board gets lost after some time or after using the flash-lamp for a few times. The true reason for the communication failure is not clear until now. It is indicated that the system is not fully electromagnetic compatible with the flash-lamp electronics in its vicinity. As a solution it might be suggested to use an optocoupler along the communication line. This way, it could be ensured that higher peak currents induced to the cable can not destroy the electronics and the two ends are galvanically separated from each other. However, this is a thought for the future and is not yet implemented.

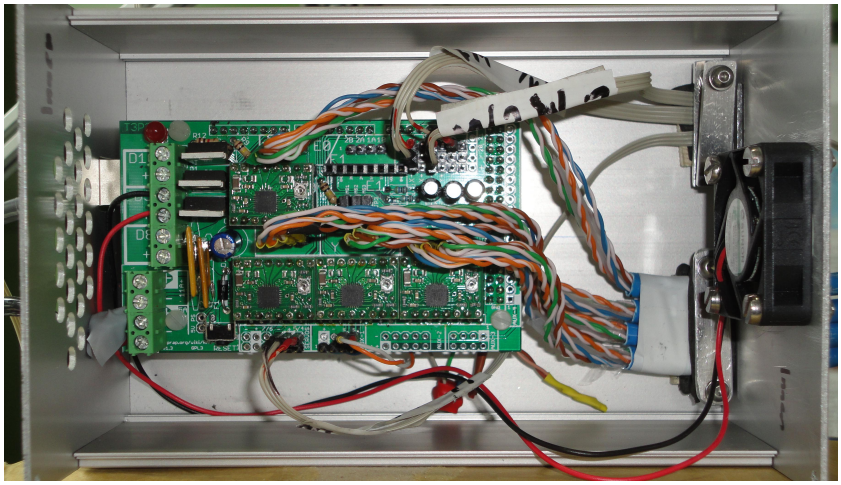

Figure 3.14.: Controller unit

[8] EMC ... **e**lectro**m**agnetic **c**ompatibility

3.2.2. Measurement-Procedure

In order to measure the Spectral Response of a module or large area cell one needs measurement-devices capable of voltage and current measurement and most important a reference solar cell with known Sr. In order to obtain the Sr it is useful to measure the complete I-V-characteristics of the module, though it is enough to measure the current only at $U = 0\ \mathrm{V}$, thus measuring the short circuit current I_{sc} [5], [6]. In addition the I_{sc} of the reference cell has to be measured. The measurement can be done with the methods existing at Photovoltaic Department of Austrian Institute of Technology GmbH in order to measure the I-V-characteristics, i.e. the system by Berger Lichttechnik, or Pasan. Of course the use of other measurement systems is possible. Basically a ampere-meter, a volt-meter and a preferably a voltage-source to set the voltage between $0\ \mathrm{V}$ and V_{oc} are required. As an alternative to the voltage-source it is possible to scan the I-V-characteristics with a variable resistor. The set-up can be seen in figure 3.16 in form of a circuit drawing. The devices have to be set-up in such a way, that the measurement is possible simultaneously at the test-module and the reference cell [5], [6].

The photovoltaic-module and the reference cell are placed inside the flasher-chamber. It is important to follow some criteria for the placement: The test-PV-module has to be placed in an area where the irradiation is the most homogeneous. The reference cell has to be next to the test-module and at a position where the irradiation is most similar to the irradiation at the module-area. Both, the reference cell and the photovoltaic-module, have to be placed at the same level to ensure the same incident irradiation on both devices.

When the system is set up for measurement the measurement can be started. This means for each optical filter (filtered wavelength) the voltage and current measurements have to be performed during one flash with the Berger-flash-lamp. Needles to say that for each measurement the desired filter position has to be moved via the software into the centre of the flash-lamp, i.e. its “filter-position”. The procedure for operating the filter-system is not explained here. A separate manual was created for that purpose. In case of the, as in this case existing, Berger or Pasan measurement systems the measurement is already triggered with the irradiation peak. In other cases, where the measurement can not be triggered with the irradiation intensity, it is indicated to measure at least for the complete time period from shortly before the flash until shortly after it. Then measurement data has to be logged with high enough number of data points. The data point chosen for evaluation should be measured during the irradiation peak, however, this is not a necessary requirement. Most important is:

the data points for the PV-module and the reference cell have to be from the same point of time to ensure measurement of both devices under the same irradiation.

After measurement the data can easily be evaluated. Taking the short circuit current I_{sc} measured at the module and the irradiance measured with the reference cell the Sr can be calculated with Eq. 2.17. In practice the area of the PV-module and the reference cell still have to be considered in the equation. Then, depending on the units of the data output from the software of the measurement-system, one of the following equations has to be used:

$$Sr_{module}(\lambda) = \frac{I_{module}}{P_{module}(\lambda)} = \frac{\bar{I}_{module}}{\bar{P}(\lambda)} \tag{3.1}$$

$$= \frac{I_{module}}{A_{module} \cdot \bar{P}(\lambda)} \tag{3.2}$$

$$= \frac{I_{module}}{A_{module} \cdot \frac{P_{ref}(\lambda)}{A_{ref}}} \tag{3.3}$$

Here the quantities $\bar{I}$ and $\bar{P}$ are the current and the irradiance per unit area. However, if the irradiance is not already automatically calculated by some software then another approach can be used. Since Eq. 3.1 is also valid for the reference cell, only that for the reference cell the irradiation is the unknown and the Sr is a known quantity, we can substitute $P(\lambda)_{ref}$ in Eq. 3.3 with a transformed Eq. 3.1 where the quantities are for the reference cell. Thus, we get:

$$Sr_{module}(\lambda) = \frac{I_{module}}{A_{module} \cdot \frac{1}{A_{ref}} \cdot P(\lambda)_{ref}} \tag{3.4}$$

$$= \frac{I_{module}}{\frac{A_{module}}{A_{ref}} \cdot \frac{I_{ref}}{Sr_{ref}(\lambda)}} \tag{3.5}$$

$$= \frac{I_{module}}{I_{ref}} \cdot \frac{A_{ref}}{A_{module}} \cdot Sr_{ref}(\lambda) \tag{3.6}$$

It is important that A_{ref} has to be only the cell area! In contrast, the area A_{module} can be including the unused space between the cells inside one module. In that case the calculated Sr is the Sr for the overall module area. If empty space is excluded then the calculated Sr is the one of the used cells in average.

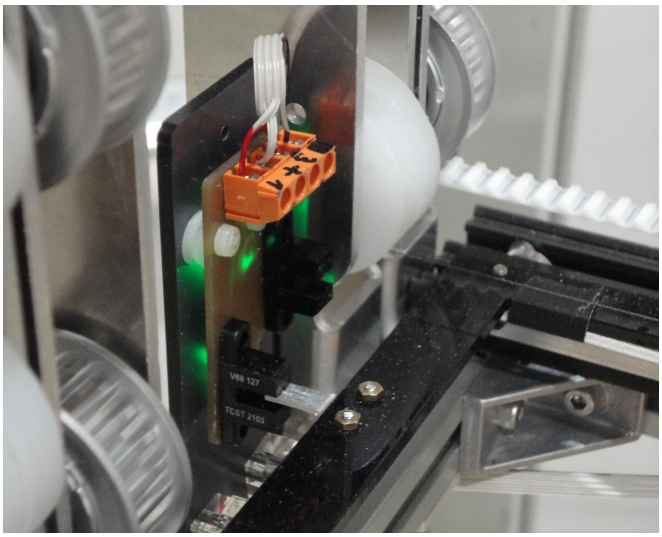

Figure 3.15.: Optical end-stop

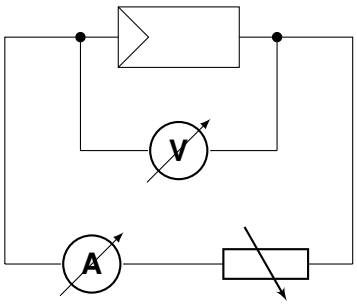

(a) Voltage sweep with variable resistor.

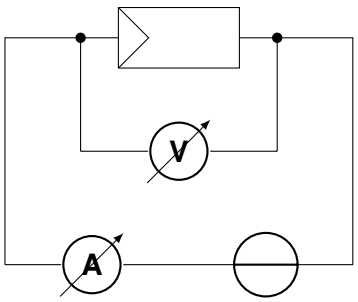

(b) Voltage sweep with voltage source.

Figure 3.16.: Two alternative circuits for measurement of I-V-characteristics and Sr: a) with variable resistor; b) with voltage source. [5], [6]

3.2.3. Potential of this System

This system, as it is, can not be used for multi-junction or thin film modules. They need bias light. In addition also modules with cells that don't have linear response to irradiation need bias as mentioned in chapter 3 on page 30. However, the possibility to upgrade this system for the use with bias light was elaborated. The idea for this upgrade is, to have two lamps illuminating the test-module from two sides. This is shown in figure 3.17. The homogeneity of the irradiance on the test-plane was estimated, since spatial homogeneity of ± 2 % has to be assured by the regulations (see page 30 in chapter 3). Through this estimation, a possible configuration for the positioning of the lamps has been calculated as well.

For this estimation several assumptions have been made for simplicity:

- The light source is a infinitely small spot.
- The light spot radiates uniform in all directions.
- Only the irradiation within an angle illuminating the module-size is considered.
- No diffuse light is considered.
- For the intensity on module-plane the formula $I \sim \frac{P}{r^2}$ is used.
- The irradiation P is set to $P = 1$W since for homogeneity only the relative intensity $\frac{\Delta I}{I_{max}}$ or more strict $\frac{\Delta I}{I_{min}}$ is important.

Below one finds a table with values for two different module sizes as well as two different positions of the two lamps relative to the module. The dimensions a and l are set, thus $a+l+a$ is equal to the inside-width of the flasher-tower. This way the lamp is considered to be still inside the construction.

h in [m]	a in [m]	l in [m]	b in [m]	$I(1+2)_{min}$ in [W/(m^2)]	$I(1+2)_{max}$ in [W/(m^2)]	ΔI in [W/(m^2)]	$\Delta I / I(1+2)_{min}$
4.00	0.85	1.20	0.60	0.1088	0.1105	0.0017	1.5844 %
4.00	0.62	1.67	0.99	0.1067	0.1105	0.0037	3.5043 %
3.40	0.62	1.67	0.99	0.1408	0.1464	0.0056	3.9580 %

Table 3.1.

So as one can see, it is possible to extend the existing system with two lamps for bias light and the homogeneity of the irradiation will most likely be within the required ± 2 % since it

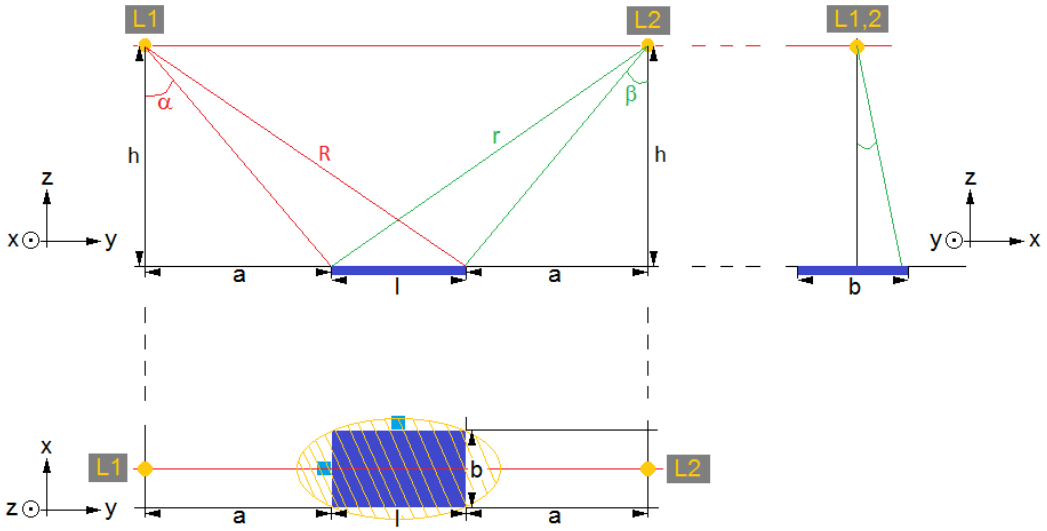

Figure 3.17.: Sketch for BIAS-light from two light spots. Included are the dimensions without values used for the calculations.

is always less then $I_{min} + 4\ \%$. However, it can not be foreseen how the situation will be when using a real light source. The requirement on a light source as bias light is not as high as for the general illumination, though this might change depending on the purpose of the bias light. If it is used for measurement of multi-junction devices and not considering non-linear response then the irradiance of the source does neither require $1000\ \frac{W}{m^2}$ nor a spectrum equivalent to AM 1.5. However, the irradiance per unit area is required to be larger than the total irradiance of the filtered light [20], [19]. Only in this case the sub-junction to be measured with filtered light will be current limiting [20], [19]. In case of multi-junction measurement, where coloured bias light is necessary, the filtering of the spectrum can easily be done with the filter foils as described in chapter 3.1.1 on page 31. Here advantage of the cheaper solution can be taken. In case where a module shows non-linear response the bias light will need to have enough power in order to bring the module close to operating condition.

For this system the measurement procedure will slightly change if extended with bias light as described above. Then it is necessary to distinguish the current-output signal from the filtered light and the bias light. One has to do two measurements for one filter wavelength. One measurement with only the bias light and a second one with the filter (being flashed with the original system) and the bias light together. From the second measurement the contribution of bias light has to be subtracted.

Chapter 4.

Measurements and Results

4.1. Expected Current-Output under filtered Spectrum

During the development phase various test measurements have been performed. The purpose was to evaluate the expected current output from a mc-Si solar cell when only a limited part of the spectrum is illuminating the cell. The test measurements followed simulations of the expected current output where the transmission spectrum of filters is assumed to be Gaussian. For this test a mc-Si cell with a size of $15.6 \times 15.6\text{cm}^2$ was used. Two different measurements have been taken:
Once a paper-box was covering a portion of the cell. The paper-box has a hole of 10.5×10.5 cm^2, almost centred, in the distance of ~ 5 cm above the solar cell (see figure 4.1, top). The paper-box prepared for housing an optical filter for the second test.
The second test was again with the paper-box, but this time the hole is covered by an optical filter with peak-wavelength of $\lambda = 850$ nm, a bandwidth of $\Delta\lambda = 40$ nm and peak-transmission of ≥ 70 %. The effective size of the filter is 6.5×6.5 cm^2 (see figure 4.1, bottom). In both cases a reference cell was used to measure the irradiance. Though, only the irradiance of the un-filtered, i.e. white, light was measured with the reference cell. Reference cell and solar cell have been at the same elevation.

In case of only the paper-box the short-circuit current was measured to be $I_{sc} = 3.55$ A. When the light spectrum is filtered then the current output of the solar cell with an illuminated area of around 42.25 cm^2 is $I_{sc} = 0.055$ A. For verification of this measurement the Sr is calculated. For this, the filtered irradiation incident on the test-solar cell is simulated, since neither the spectrum nor the true irradiance are known. As the transmission of the filter is unknown as well, the transmission is assumed to be Gaussian with maximum transmission of

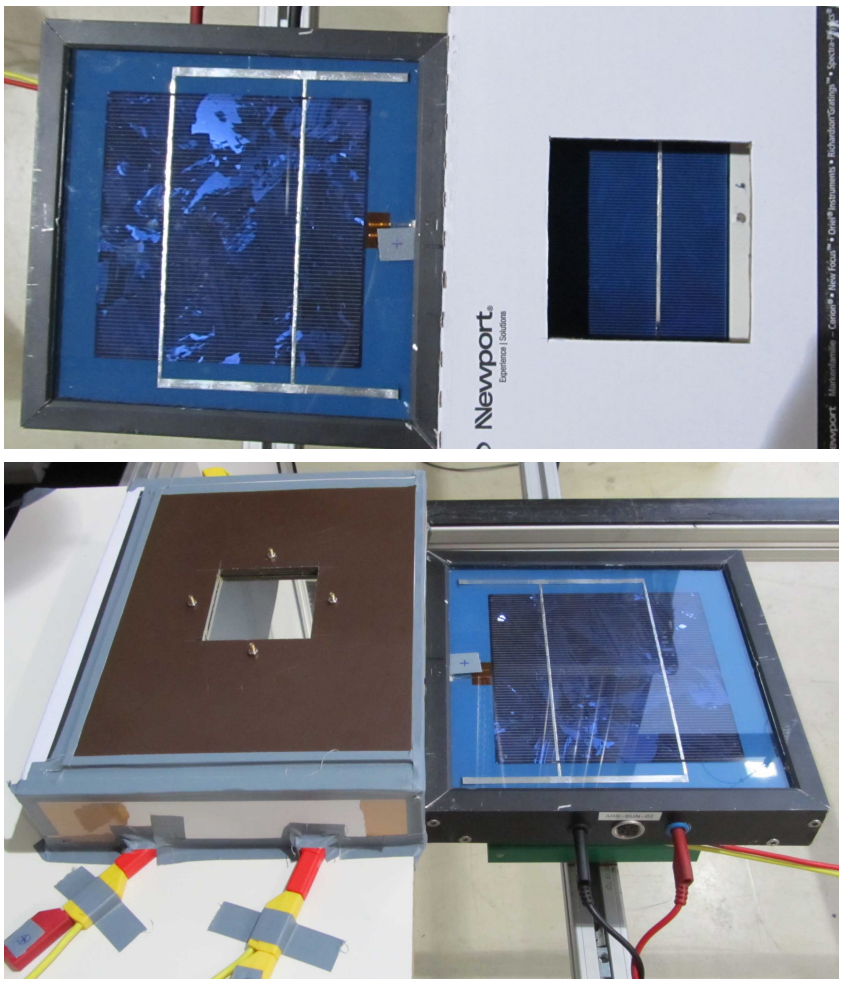

Figure 4.1.: Test-setup for measuring expected current output under filtered light spectrum. Top: Limited cell-area without filter; Bottom: Limited cell-area with filter

$70\ \%$ and a transmission spectrum is simulated, too. The simulated irradiance after filtering is $28.6442\ \frac{\mathrm{W}}{\mathrm{m}^2}$. Assuming that the current is only produced by the cell-area illuminated, thus the area of $42.25\ \mathrm{cm}^2$, then Sr is calculated as $Sr = \frac{I}{A \cdot P}$. The result is $Sr(850\ \mathrm{nm}) = 0.454\ \frac{\mathrm{A}}{\mathrm{W}}$. The correct value for this cell is unknown, but the result is plausible. Therefore it can be assumed that for single cells a current in magnitude of $\frac{1}{100}$ A can be expected and that a current as low as this can be measured with the existing measurement equipment for I-V-characteristics measurement. In addition it can be derived that for PV-modules higher currents are expected.

4.2. Spatial Homogeneity

After assembling the Sr-measurement system the spatial homogeneity of a filtered light beam has to be verified and the size of an area complying with the requirements in the standard has to be determined. This measurement is not only required, but also interesting since the influence of the filter-holders (see picture 3.8 on page 42) on the spatial irradiation distribution was unknown. For this measurement the irradiation was measured over the complete area within the housing for the measurement. Two measurements have been taken, one in the state for I-V-measurements, i.e. without a filter below the lamp, another one with a filter-position moved below the lamp, i.e. the Sr-measurement configuration. In the latter case a filter-position without optical filters installed was chosen in order to measure at full irradiation. The spatial distribution of irradiation is obviously expected to be un-influenced when using optical filters. The result is shown in figure 4.2. In the case with a filter inside, the area with homogeneity of $100\ \%\ \pm 2\ \%$ (see figure 4.2b) is very limited and shifted to the front of the housing. It seems that the ribs of the filter-carriers don't have influence on the spatial irradiance distribution. But since the filter area is elongated in width and not squared, at the front and back of the housing irradiance is decreased. This is because the corresponding part of the lamp is partially covered by the aperture and only the portions on the left and right side of the lamp, being exactly above the filter-pieces on left and right of the total filter area, give the main contribution. The area usable for measurements according to the homogeneity requirements by the normative regulations is limited to only 475×660 mm. This is only half the size of small modules. Choosing the area in the centre one gets a much wider area available, but with only 420 mm in height. Looking at the third graph (figure 4.2c) the tolerance is increased to $100\ \%\ \pm 5\ \%$. In that case the usable area increases to 2255×1105 mm which is clearly enough for use with PV-modules of larger size.

4.3. Spectral Response-Measurement: System Verification

After the Sr-measurement system was assembled and the filter-positioning system was tested for functionality, test-measurements of two PV-modules with known Sr have been performed. The purpose is to verify that with this system Sr of PV-modules can be measured, to evaluate necessary or recommended improvements and to detect errors in the measured data. For the measurements both equipments, the one by Berger and by Pasan, have been used to measure the I-V-characteristics of PV-modules. The current used to evaluate the Sr, but due

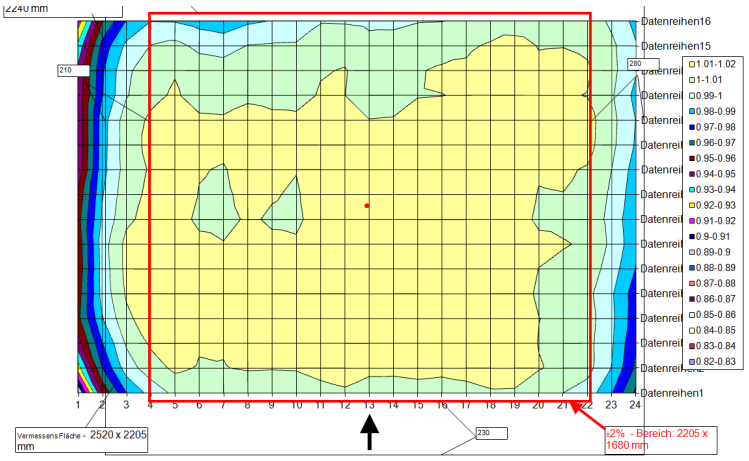

(a) Homogeneity without filter and aperture. Standardised within ± 2 %.

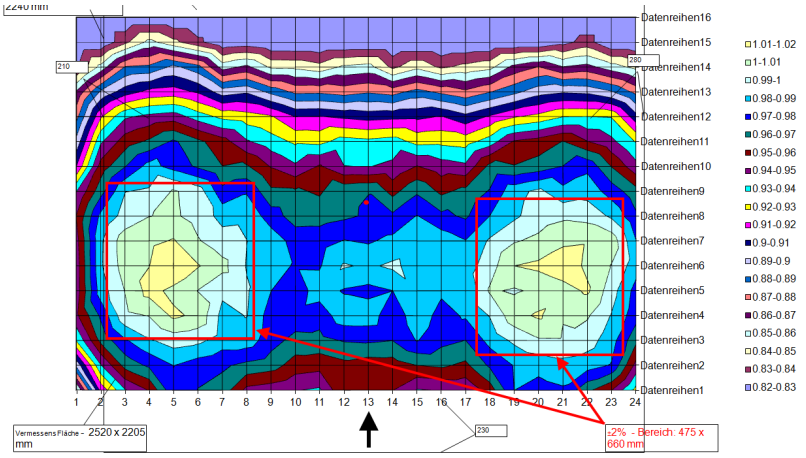

(b) Homogeneity with filter and aperture. Standardised within ± 2 %.

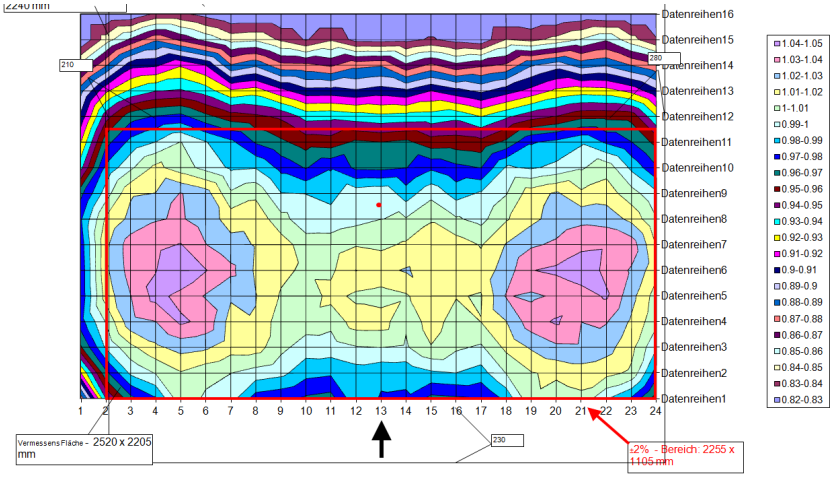

(c) Homogeneity with filter and aperture. Standardised within ± 5 %.

Figure 4.2.: Homogeneity of irradiation for three configurations inside the lamp-housing. The irradiation is standardised, thus the maximum irradiation measured corresponds to 102 % (for the case with ± 2 %) and 105 % respectively.

to problems with the communication cable for controlling the filter-position of the modules is the short circuit current as stated in chapter 2.2. All together two modules have been measured, one module with CdTe-cells by First Solar and the second one with mono-crystalline Si-cells by Kioto. It was desired to measure at least one more module with known Sr and use different measurement devices for comparison. But due to problems with the communication cable for controlling the filter-position and a lack of time and resources, it was not possible to do more measurements for this work. The module and a reference cell are placed rather in the front of the housing as seen in figure 4.3. This is to have the module in the area with highest irradiation and in the zone where spatial homogeneity is the best. However, the reference cell is in an area which is already a bit outside this area (see figure 4.2b).

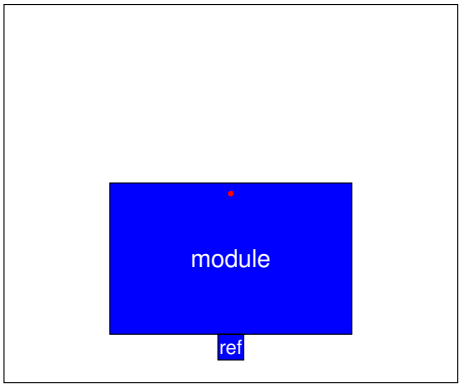

Figure 4.3.: Placement of the PV-module and the reference cell inside the measurement housing. Not to scale!

4.3.1. Spectral Response: Kioto-module

This PV-module is produced by Kioto, type `KPV_PE_ME_250W`. The size of this module is 167×99 cm^2, with an array of 6×10 solar cells which are all connected in series. The solar cells are c-Si solar cells. The total module area is 1.6533 m^2. The Sr of this module is unknown. The measurement was the first done with this system and performed quickly to get a first result showing that the system is working in general. The measurement of the I-V-characteristics was performed for the filters with peak-wavelengths at 500 nm and 700 nm.

The results from the measurements are shown in the table below:

λ [nm]	$\Delta\lambda$ [nm]	$P\left[\frac{\mathrm{W}}{\mathrm{m}^2}\right]$	I_{sc} [A]	T [°C]
500	20	688	4.374	24.8
700	20	711	4.415	24.8

As one can see from the measurement data, the irradiation measured is much higher than the irradiation expected behind bandpass-filters with a bandwidth of 20 nm. In fact when checking the filter position visually after the measurement, the filter carriage appeared to be stuck in a position without optical filters. This explains the high irradiation. Therefore, the Sr can not be evaluated for this PV-module. Still this circumstances might have an impact on further measurements. When analysing the data from the homogeneity measurement with a filter position without filters inside and the aperture moved inside, the following irradiance was measured inside the relevant area for the module and the reference cell: max. $823.3\ \frac{\mathrm{W}}{\mathrm{m}^2}$, min. $756.0\ \frac{\mathrm{W}}{\mathrm{m}^2}$ with a homogeneity of $\pm 4.26\ \%$. In average the irradiance is $787.6\ \frac{\mathrm{W}}{\mathrm{m}^2}$. Compared to this value, during I-V-measurements of the Kioto-PV-module the irradiance without filters was in average $1015\ \frac{\mathrm{W}}{\mathrm{m}^2}$ out of three measurements. This shows analogy to the Kioto-module measurement.

4.3.2. Spectral Response: First Solar-module

This PV-module is the type `FS270` produced by First Solar. The size of this module is 120×60 cm^2, with 116 solar cells connected in series. The module is made of CdTe solar cells. The total module area is 0.72 m^2. The Sr of this module is already measured by another institute and is available for comparison with this measurement result. It can be seen in figure 4.4. The measurement of the I-V-characteristics was performed only for the filter with peak-wavelengths at 700 nm. More measurements have not been possible due to the technical problems with moving the filters, as described at the beginning of chapter 4.3.

This time the filter was correctly positioned and the measurement is usable. The results from the measurements are shown in the table below:

Measurement	λ [nm]	$\Delta\lambda$ [nm]	$P\left[\frac{\mathrm{W}}{\mathrm{m}^2}\right]$	I_{sc} [A]	T [°C]
No. 1	700	20	37.1	0.0407	–
No. 2	700	20	54.7	0.0624	–

Calculating the Sr using equation 3.2 (on page 50) we get for measurement No. 1 $Sr(700\,\text{nm}) = \frac{0.0407\ \text{A}}{(0.72\ \text{m}^2 \div 116)\cdot 37.1\ \frac{\text{W}}{\text{m}^2}} = 0.177\ \frac{\text{A}}{\text{W}}$ and for measurement No. 2 $Sr(700\,\text{nm}) = 0.184\ \frac{\text{A}}{\text{W}}$. The total area of the module is divided by 116 because the cells are series-connected, thus the current is limited to the current of the weakest solar cell. However, the Sr is supposed to be around $0.503\ \frac{\text{A}}{\text{W}}$. The Sr measured here is smaller than expected by a factor of ≈ 3.

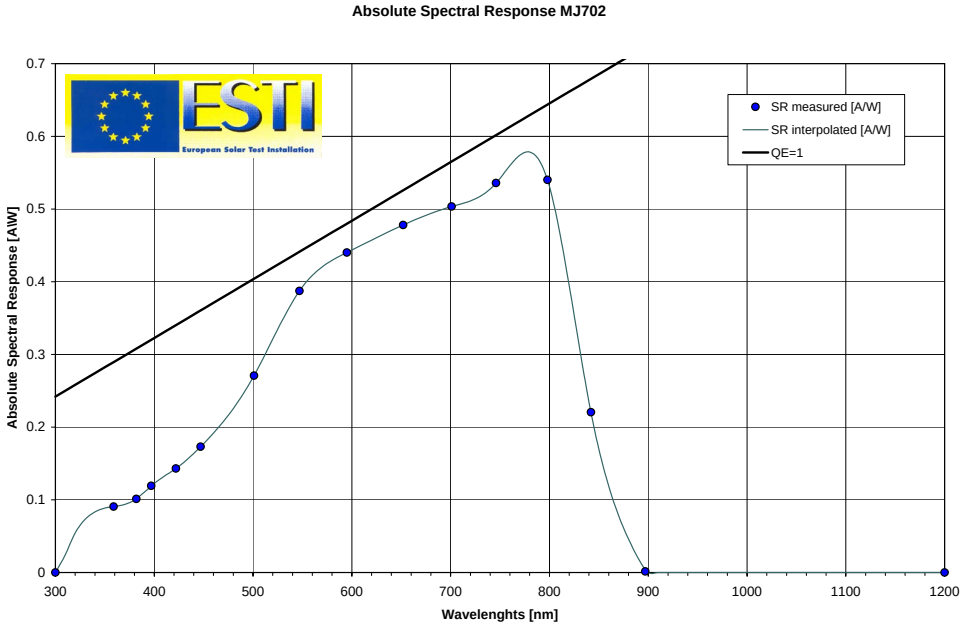

Figure 4.4.: Spectral response of a CdTe test-module. Measured by ESTI (European Solar Test Installation) laboratory in 2009. [7]

Therefore an analysis of the error is necessary. One of the errors is because the irradiance was calculated by the measurement-software under assumption of a scaled standard spectrum. I.e. the irradiance is calculated by multiplying the measured voltage (corresponding to the current output) of the reference cell with a calibration constant. Since it is extremely difficult to reconstruct the real spectrum, this error remains. The problem with the spectrum is, that is it a combination of possibly diffuse white light and the filtered light with peak-wavelengths at 700 nm and a bandwidth of 20 nm. During a further attempt to estimate a better result, it will be referred to this issue again. Starting point for the attempt to correct the result is the irradiance measured during homogeneity measurement and the fact, that the simulation of expected irradiance after optical filters reveals much lower irradiance than the measured one. Here important is the irradiance along one cell, especially the lowest irradiance since the exposed cell will be the current-limiting one. Then the irradiance with a filter-position inside, but without actually filters, in the area in question is in average $P_{av} = 783\ \frac{\text{W}}{\text{m}^2}$. The expected irradiance after optical filters is $\bar{P}(700\,\text{nm}) = 14.9\ \frac{\text{W}}{\text{m}^2}$ (originated

from $1000\ \frac{\mathrm{W}}{\mathrm{m}^2}$ un-filterd). Thus, the filtered irradiance originated from P_{av} will correspondingly scaled to $P(700\ \mathrm{nm}) = 11.7\ \frac{\mathrm{W}}{\mathrm{m}^2}$. From the difference between the measured and the expected irradiance one can derive the portion of diffuse white light with $P_{diff} = P_{meas} - P(700\ \mathrm{nm})$. Only problem here is, that everything following will be related to the irradiance at the homogeneity measurement. But the irradiance of the flash lamp before filters is most likely at different levels. This can be seen at the irradiance-values during this I-V-characteristics measurement. They differ by a factor of 1.5. Further, the short circuit current from diffuse white light can be estimated by relating it to the standard conditions (STC): $I_{sc,diff} = \frac{I_{sc,STC}}{P_{STC}} \cdot P_{diff}$. Then the short circuit current from filtered light is $I_{sc}(700\ \mathrm{nm}) = I_{sc,meas} - I_{sc,diff}$. Finally the Sr can be calculated using $Sr(\lambda) = \frac{I_{sc}}{A \cdot P(\lambda)}$. In this case we get for measurement No. 1 $Sr(700\ \mathrm{nm}) = 0.169\ \frac{\mathrm{A}}{\mathrm{W}}$ and for measurement No. 2 $Sr(700\ \mathrm{nm}) = 0.179\ \frac{\mathrm{A}}{\mathrm{W}}$. This shows that the assumed correction of the measurement did not bring an improvement.

Chapter 5.

Discussion and Outlook

5.1. Error Estimation and Discussion

Looking at the result of the Sr measurement a detailed error analysis with the value and type of each error is not reasonable. One of the reasons is, that the overall error can be deduced from the result in chapter 4.3.2 to be around $63\ \%$ ($= \frac{Sr - Sr_{meas}}{Sr}$, which is very high and far larger than the error of the measurement devices. Other reasons are the uncertainties due to several, possibly important, issues which are named and described below. The contribution of those uncertainties to the error can not be told without further investigation.

- **Pollution with white light:** The gaps where white, un-filtered light can pass into the housing of the measurement have not yet been covered. There are many such gaps that can be closed. In addition there is a gap that is hard to close: During mounting the filter-system on the existing construction it appeared that one of the planned changes at the construction is impossible. The consequence is, that the aperture had to be narrowed, thus a gap between the aperture-carriage and the lamp-housing-aperture appeared. From there white light is most likely to pass to the PV-module.

- **Unknown spectrum at module-level:** Especially because of the unknown quantity of white spectrum irradiance it is advised to perform a measurement of the spectrum. Another reason for this measurement is, that the spectrum of the filtered light is very likely to be shifted or broadened as the incident light from the lamp itself is not only perpendicular to the optical filters. This measurement should also show spatial variation of the spectrum along the complete measurement plane.

- **Sr of the reference cell:** It is necessary to use the known Sr of the reference cell for the calculation of the test-module's Sr. The use of calculated irradiance via a calibration factor is not recommended. In this case the calculation will have to be extended by considering the Sr for each wavelength of the finite bandwidth of filtered light in order to reach a minimum error.

- **Measurement devices:** By considering the Sr of the reference cell it will be necessary to measure the current output I_{sc} with a system as shown in figure 3.16b) on page 51. However, each measurement device should be on its own and a combined system, like the here used Pasan or Berger system, is not recommended. Then all measurement data is easy accessible for evaluation. In case of the used measurement equipment the current-output data of the reference cell is not available.

- **Data average:** Since one has to do several measurements of the same condition and then calculating the average to reduce errors, it has to be suggested to measure the output current of the module and the reference cell for one setting of load, i.e. voltage, during a single flash. Then the currents during a period of stable irradiation can be averaged. This should be preferred to doing several flashes, measuring the I-V-characteristics and calculating the average of those results.

- **Voltage-dependent Sr of CdTe:** CdTe as well as some other solar cell types are reported to have the Sr depending on the voltage. The origin is actually that the collected current is depending on the voltage at the solar cell [20] (p. 824). In that case the measurement can not necessarily be performed at $V = 0$ V. In this case applies the same procedure as suggested for multi-junction devices. A forward bias voltage is applied and swept between 0 V and V_{oc} until Sr becomes maximum [20] (p. 825).

- **Effect of low irradiance on the Sr:** It might be possible that the Sr is lower at low irradiance, thus a measurement without bias light. This is because at very low irradiance the produced photo charge carriers are getting trapped before they can be extracted at bus-bars of contacts. Only at a bit higher irradiation those traps are filled and the majority of the produced charge carriers contribute to the current output [8]. In our case for the Sr-measurement at 700 nm the Sr of a mc-Si solar cell is likely to exhibit such an effect, but will be reduced by only about 3 % or less [8]. For CdTe solar cells low irradiance can cause various effects on the QE or Sr as written in [27]. Again the trapping of charge carriers is the reason. How this affects the measurement performed for this work can not be assessed.

- **Bad test-module sample:** It could also be considered that unfortunately the used PV-module is a sample with unknown failure. Just one improper working cell inside this module can result in a Sr-value that is unequal to the expected value. This can be because this module consists of only series connected cells, where the worst performing one is current limiting and thus determines the performance of the whole PV-module. This suggestion can be supported by the analysis of the reference solar cell as below.

  Analysis of the reference cell: As the Sr-data for the reference cell is unavailable, data from other publications for polycrystalline silicon solar cells are taken. The Sr-data was taken from [8], [9], [10], [11]. Then the short circuit currents at $1000\ \frac{\mathrm{W}}{\mathrm{m}^2}$ (STC) and for light filtered with the used filter at 700 nm was calculated from that data. From those values the estimated short circuit currents under condition of the measurement in chapter 4.3.2 was calculated, i.e. a white diffuse light of $P_{diff} = 43.0\ \frac{\mathrm{W}}{\mathrm{m}^2}$ and filtered content with $P(700\ \mathrm{nm}) = 11.7\ \frac{\mathrm{W}}{\mathrm{m}^2}$. The plot of this data can be seen in figure 5.1. The measured $I_{sc}(700\ \mathrm{nm})$ of the reference cell was calculated using the irradiance calculated by the measurement software and the known calibration value as well as the shunt-resistance for current-to-voltage signal conversion. The comparison of this value ($I_{sc}(700\ \mathrm{nm}) = 0.42$ A) with the plotted data shows that the measured value might be $10\ \%$ below expectation. However, calculating the current resulting only from the filtered light and not the white diffuse light contribution there are two results, one by scaling down this current by $10\ \%$ as above as well and the other result without that scaling: the Spectral Response is in the first case $0.44\ \frac{\mathrm{A}}{\mathrm{W}}$ and in the latter case $0.48\ \frac{\mathrm{A}}{\mathrm{W}}$. The latter value complies relatively good to the Spectral Response-data used for this rough evaluation. Thus, it provides evidence that the measurement was performed correctly and most of the error ($63\ \%$ as stated above) is due to poor module performance and are not actual measurement errors.

5.2. Outlook

A prototype for Sr-measurement of full-size PV-modules has been planned and constructed. In addition this system is integrated into an existing I-V-measurement system at AIT GmbH. After performing test measurements of different kinds, there appears still improvement to be done as well as potential extensions to enhance the use of the system. Yet, the system is not capable to perform measurements with the purpose of certification according to the

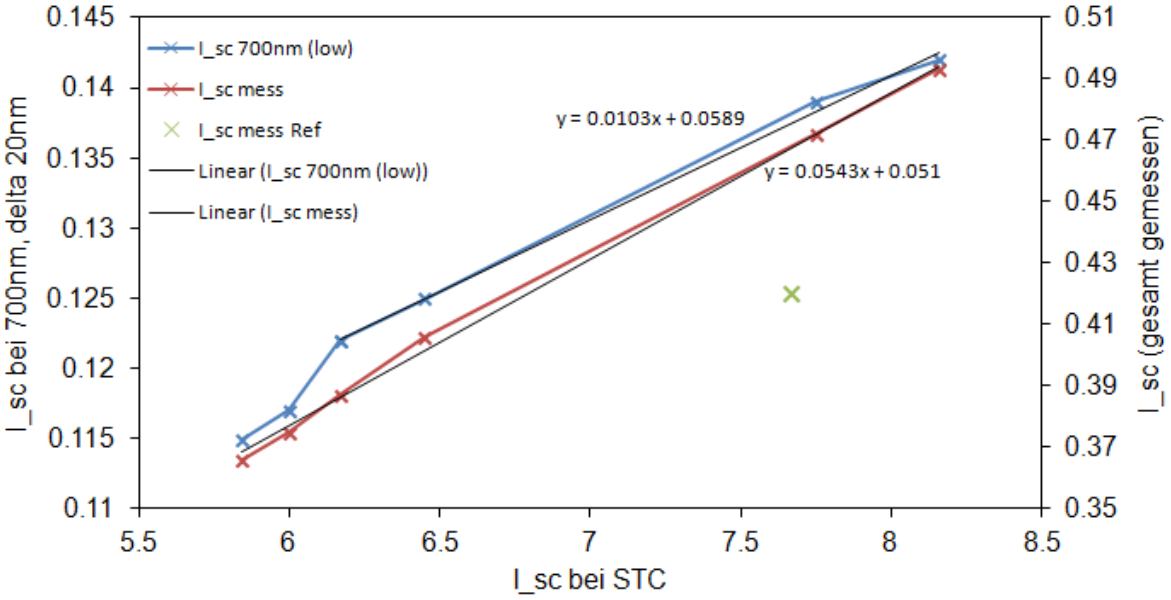

Figure 5.1.: Plot of short circuit currents of mc-Si solar cell with different Spectral Response. Left axis: I_{sc}, when filtered with 20 nm bandwidth at 700 nm and a total irradiance of $11.7\ \frac{\mathrm{W}}{\mathrm{m}^2}$, against I_{sc} at STC; right axis: I_{sc}, when filtered as before plus a diffuse white light of $43\ \frac{\mathrm{W}}{\mathrm{m}^2}$, against I_{sc} at STC. The Sr-data originates from [8], [9], [10] and [11].

normative regulations on Sr measurement. The possible or required improvements are as follows: The problem with the communication between the PC and the filter-positioning controller has to be solved. This is important to position the filters correctly below the lamp and it will improve the usability. Second recommendation, as already told before, is to use separate volt-meter and ampere-meter for better accessibility of the measurement data. Further advantages are that different bias voltages can be set and the device can be selected according to the required measurement range. This choice should be preferred to the standard devices provided or offered by Berger or Pasan. Another issue to be solved is the homogeneity. So far the area with ± 2 % homogeneity according to the normative regulation is very limited and only suitable for very small modules. With the intention to be able to certify PV-modules according to the regulations, this area has to be extended. For this, different ways of partially covering the optical filters have to be tested, or other solutions need to be found. The last and most important issue is the pollution with diffuse white light inside the measurement housing. For this all or at least the most disturbing gaps at the lamp-housing need to be covered. Another thought might be a differential measurement procedure to correct measurement results. For this procedure one slot in each carriage with filters needs to be 100 % light-blocking. Then one measures the different filter positions and the blocking

positions and from the difference in the signal one can deduce the signal originating from the narrow-bandwidth spectrum. Only disadvantage in this case is, that for each position several flashes are necessary in case the irradiation varies with each flash. Then one needs to calculate an average value from the measurements of each filter/blocking position respectively. Another disadvantage is that altogether three filter-positions will get lost, thus, three wavelength steps are missing for the Sr measurement.

The one extension of this system in the future is to extend its capability for multi-junction devices or devices with non-linear response. For this, it needs to be extended with coloured or white bias light as discussed in chapter 3.2.3. However, the measurement procedure will have to be changed since the difference between bias and filtered signal needs to be retrieved from the measurement.

One additional thought has to be mentioned here: Due to the advantages of a bandstop-filter as described in chapter 3.1.4, the use of those are still interesting for application in Sr measurement and in favour. A interesting question is the signal-to-noise ratio in the case of using bandstop-filters compared to using bandpass-filters. This might be important as in the system of this work the noise can not be reduced by chopping the monochromatic light and using a lock-in amplifier for the measurement of the current. When the short light pulse would be chopped and the time period of illumination becomes too short, then an additional error appears in the result. This is due to the finite response time of the PV-device [28], i.e. a PV-device needs some time from switching on a light source until the current output due to illumination reaches its maximum. The upper recommended chopping frequency of 100 Hz ([20], p. 830) results in a period length of 10 ms, which is as long as a pulse length of the flash lamp used for this work. Despite having the system built with bandpass filters, the system can easily be changed. Simply the filters have to be exchanged since the rest of the components or the construction remains the same and the filters usually can be purchased with the same dimensions. Then the modules are illuminated at almost exactly 1-sun irradiation, thus at operation condition and the measured current is much higher. Only one will have to think about a new way to measure the Sr of multi-junction devices.

Chapter 6.

Summary

As an important part of this work, several possibilities for achieving quasi-monochromatic light have been evaluated and the most promising ones have been shortly discussed in this work. Based on those results, a Spectral Response-measurement system has been developed, designed and built, including necessary, non-standard components and pieces. This phase is the second important and biggest part for this project. The developed Sr-measurement system is based on optical bandpass filters, used for getting quasi monochromatic light. The system and its components have been explained more detailed in this work. The goal to integrate the system inside an existing vertical I-V-measurement system is achieved and the possibility to measure commercial sized PV-modules has its limits. Achieving a large area with homogeneous irradiation within ± 2 % is difficult with this set-up as it is and is not achieved. Only very small modules can be measured under that condition. In addition, leaking white light is most likely disturbing the Spectral Response-measurement, thus overcoming any other measurement error. Therefore, the system can not yet be used for a serious Spectral Response-measurement. However, this system is a first prototype which has to be and can be improved. Furthermore, this system has potential to be extended, e.g. for use with other PV-module technology such as multi-junction devices after installing coloured bias light.

Appendix A.

Physical Constants and Units

$QE(\lambda)$	quantum efficiency	[%] or [1]
n_q	number of charged particles	
n_{ph}	number of photons	
$Sr(\lambda)$	spectral response	$\left[\frac{\mathrm{A}}{\mathrm{W}}\right]$
I	electrical current	$[\mathrm{A}]$
I_{sc}	short circuit current	$[\mathrm{A}]$
$j(\lambda)$	output current at λ	$\left[\frac{\mathrm{A}}{\mathrm{nm}}\right]$
U	voltage	$[\mathrm{V}]$
U_{oc}	open circuit voltage	$[\mathrm{V}]$
E_g	bandgap energy	$[\mathrm{eV}]$
λ	wavelength	$[\mathrm{nm}]$
λ_0	central peak wavelength	$[\mathrm{nm}]$
$\Delta\lambda$	bandwidth at FMHW	$[\mathrm{nm}]$
$P(\lambda)$	irradiance	$\left[\frac{\mathrm{W}}{\mathrm{m}^2}\right]$
$p(\lambda)$	spectral irradiance at λ	$\left[\frac{\mathrm{W}}{\mathrm{nm}}\right]$
h	Planck constant	$= 6.626 \cdot 10^{-34}\ \mathrm{Ws}^2 = 4.136 \cdot 10^{-15}\ \mathrm{eVs}$
k_B	Boltzmann constant	$= 1.3807 \cdot 10^{-23}\ \frac{\mathrm{Ws}}{\mathrm{K}} = 8.617 \cdot 10^{-5}\ \frac{\mathrm{eV}}{\mathrm{K}}$

c	speed of light	$= 2.998 \cdot 10^8 \ \frac{\mathrm{m}}{\mathrm{s}}$
q	elementary charge	$= 1.6 \cdot 10^{-19} \ \mathrm{As}$

Appendix B.

Abbreviations

Sr Spectral Response

QE Quantum Efficiency

PV photovoltaic

LED Light Emitting Diode

OD optical density

Appendix C.

Bibliography

[1] downloaded on 18. May 2011. http://upload.wikimedia.org/wikipedia/commons/f/fa/Pn-junction-equilibrium-graphs.png.

[2] Photovoltaic devices - part 8: Measurement of spectral response of a photovoltaic (PV) device, 1998. IEC 60904-8, 2nd edition.

[3] Seoul Semiconductor. Technical Data Sheet - Z-power LED, February 2011. Document No. SSC-QP-7-07-24, Rev. 10, p. 16.

[4] Edmund Optics Inc. Coating Curve. http://www.edmundoptics.com/optics/optical-filters/notch-filters/od-4-notch-filters/67109.

[5] Keith Emery. Current-Voltage Measurements, chapter 18.3, pages 797–840. John Wiley & Sons, Ltd, 2nd edition, 2011.

[6] Keithley Instruments, Inc. Making I-V and C-V Measurements on Solar/Photovoltaic Cells Using the Model 4200-SCS Semiconductor Characterization System, October 2007. Application Note Series, Number 2876.

[7] ESTI (European Solar Test Installation) laboratory. Absolute spectral response mj702. unpublished result of Spectral Response test measurement by ESTI laboratory of the Joint Research Centre of the European Union, 2009.

[8] Dieter Meissner. Solarzellen: physikalische Grundlagen und Anwendungen in der Photovoltaik. Vieweg Verlag, 1993.

[9] J. Metzdorf, W. Möller, T. Wittchen, and D. Hünerhoff. Principle and application of differential spectroradiometry. Metrologia, 28:247–250, 1991.

[10] J. Metzdorf, S. Winter, and T. Wittchen. Radiometry in photovoltaics: calibration of reference solar cells and evaluation of reference values. Metrologia, 37:573–578, 2000.

[11] N. H. Reich et al. Weak light performance and spectral response of different solar cell types. http://www.ecn.nl/docs/library/report/2005/rx05034.pdf.

[12] K. Emery and National Renewable Energy Laboratory (U.S.). Photovoltaic Spectral Responsivity Measurements. National Renewable Energy Laboratory, 1998. http://books.google.at/books?id=V0ZBOAAACAAJ.

[13] C.R. Osterwald. Standards, Calibration, and Testing of PV Modules and Solar Cells, chapter III-2, pages 1045–1070. Academic Press, 2nd edition, 2012.

[14] J. Nelson. The Physics of Solar Cells. Imperial College Press, 2009.

[15] A. Goetzberger, J. Knobloch, and B. Voß. Crystalline Silicon Solar Cells. Wiley & Sons, 1998.

[16] St.R. Wenham, M. Green, M.E. Watt, and R. Corkish. Recombination of Electrons and Holes, chapter 3.6, pages 74–90. Wiley-VCH Verlag, 2nd edition, 2009.

[17] T. Markvart and L. Castañer. Principles of Solar Cells Operation, chapter IA-1, pages 7–31. Academic Press, 2012.

[18] St.R. Wenham, M. Green, M.E. Watt, and R. Corkish. The behaviour of solar cells, chapter 3, pages 43–55. Centre for Photovoltaic Engineering, 2nd edition, 2006.

[19] Mauro Pravettoni. To bias or not to bias? an "how-to" guide for spectral response measurements of thin film multi-junction photovoltaic modules. MRS Proceedings, 1426:81–86, 2012. presubmission Version, ManuscriptID: 1260936.R1.

[20] Keith Emery. Measurement and Characterization of Solar Cells and Modules, chapter 18, pages 797–840. John Wiley & Sons, Ltd, 2nd edition, 2011.

[21] J. Sutterlüti, S. Janki, A. Hügli, J. Meier, and F. P. Baumgartner. Mapping of the local spectral photocurrent of monolithic series connected a-Si:H p-i-n thin film solar modules. In 21st European Photovoltaic Solar Energy Conference Proceedings, 2006. Presented at the 21st EUPVSEC, 4. - 8. September, Dresden, Germany.

[22] C. Schmid, D. Habermann, C. Buchner, G. Hahn, A. Herguth, B. Raabe, S. Scholz, H. Haverkamp, and R. Nissler. Influence of spectral mismatch, cell reflection properties

and IQE on the efficiency measurement. In 26th European Photovoltaic Solar Energy Conference Proceedings, pages 1555 – 1557, 2011.

[23] D. Domine, M. Pravettoni, A. Virtuani, D. Pavanello, M. Bernasocchi, and G. Friesen. Spectral characterization tools used at SUPSI for indoor performance measurement of single and multi-junction photovoltaic modules. In 26th European Photovoltaic Solar Energy Conference Proceedings, pages 3450 – 3453, 2011.

[24] S. Kohraku and K. Kurokawa. New methods for solar cells measurement by LED solar simulator. In Photovoltaic Energy Conversion, 2003. Proceedings of 3rd World Conference on, volume 2, pages 1977 –1980 Vol.2, May 2003.

[25] LEE filters. Spectral Charts, August 2009. http://www.leefilters.com/lighting/lighting-resources.html.

[26] BERGER Lichttechnik GmbH & Co. KG. PSS 30 - Solar Simulator Device, December 2012. http://www.bergerlichttechnik.de/resources/Berger_Lichttechnik_PSS_30.pdf.

[27] M. Gloeckler and J. R. Sites. Apparent quantum efficiency effects in CdTe solar cells. Journal of Applied Physics, 95(8):4438–4445, 2004.

[28] K. Emery and National Renewable Energy Laboratory (U.S.). Uncertainty analysis of certified photovoltaic measurements at the National Renewable Energy Laboratory [electronic resource] / K. Emery. National Renewable Energy Laboratory Golden, CO, 2009. http://www.nrel.gov/docs/fy09osti/45299.pdf.